![AMERICAN SOCIETY FOR MICROBIOLOGY | mBio logo]

Spatial and Functional Organization of Human Papillomavirus Replication Foci in the Productive Stage of Infection

Simran Khurana,[a] Tovah E. Markowitz,[b,c] Juraj Kabat,[d] (ID) Alison A. McBride[a]

[a]Laboratory of Viral Diseases, National Institute of Allergy and Infectious Diseases, National Institutes of Health, Bethesda, Maryland, USA
[b]NIAID Collaborative Bioinformatics Resource (NCBR), National Institute of Allergy and Infectious Diseases, National Institutes of Health, Bethesda, Maryland, USA
[c]Advanced Biomedical Computational Science, Frederick National Laboratory for Cancer Research, Frederick, Maryland, USA
[d]Biological Imaging Section, National Institute of Allergy and Infectious Diseases, National Institutes of Health, Bethesda, Maryland, USA

ABSTRACT The life cycle of human papillomavirus (HPV) depends on keratinocyte differentiation as the virus modulates and takes advantage of cellular pathways to replicate its genome and assemble viral particles in differentiated cells. Viral genomes are amplified in nuclear replication foci in differentiated keratinocytes, and DNA repair factors from the DNA damage response signaling pathway are recruited to replicate viral DNA. The HPV genome is associated with cellular histones at all stages of the infectious cycle, and here, we show that the histone variant macroH2A1 is bound to the HPV genome and enriched in viral replication foci in differentiated cells. macroH2A1 isoforms play important roles in cellular transcriptional repression, double-strand break repair, and replication stress. The viral E8^E2 protein also binds to the HPV genome and inhibits viral replication and gene expression by recruiting NCoR/SMRT complexes. We show here that E8^E2 and SMRT also localize within replication foci, though independently from macroH2A1. Conversely, transcription complexes containing RNA polymerase II and Brd4 are located on the surface of the foci. Foci generated with an HPV16 E8^E2 mutant genome are not enriched for SMRT or macroH2A1 but contain transcriptional complexes throughout the foci. We propose that both the cellular macroH2A1 protein and viral E8^E2 protein help to spatially separate replication and transcription activities within viral replication foci.

IMPORTANCE Human papillomaviruses are small DNA viruses that cause chronic infection of cutaneous and mucosal epithelium. In some cases, persistent infection with HPV can result in cancer, and 5% of human cancers are the result of HPV infection. In differentiated cells, HPV amplifies viral DNA in nuclear replication factories and transcribes late mRNAs to produce capsid proteins. However, very little is known about the spatial organization of these activities in the nucleus. Here, we show that repressive viral and cellular factors localize within the foci to suppress viral transcription, while active transcription takes place on the surface. The cellular histone variant macroH2A1 is important for this spatial organization.

High oncogenic-risk human papillomaviruses (HR-HPVs), such as HPV16, 18, and 31, are the causative agents of anogenital and oropharyngeal cancers (1). In addition, infection with some HPV types from the *Betapapillomavirus* genus may predispose to squamous cell skin cancer (2). HPVs infect the actively proliferating basal layer of keratinocytes to establish a persistent infection (3). There are three stages of DNA replication in the HPV viral life cycle. First, there is an initial burst of viral DNA replication in the initial host cell, and the viral genome becomes established as a low copy number

extrachromosomal plasmid. During the second stage, established genomes are replicated and partitioned along with host DNA to daughter cells. Finally, when the infected cells differentiate, the viral genome amplifies to very high levels (4). During the productive phase of the HPV viral life cycle, repair factors from the ATM and ATR (ataxia-telangiectasia mutated and Rad3 related) DNA damage signaling pathways are hijacked by HPV to amplify viral DNA in nondividing cells (5).

The viral E1 and E2 proteins initiate viral DNA replication, and in addition, E2 regulates transcription and facilitates partitioning of viral genomes (6). E1 is a helicase that unwinds the viral origin and recruits host cellular factors to the viral replication foci, and coexpression of E1 and E2 proteins leads to the formation of nuclear foci that recruit DNA damage factors, including pATM, pChk2, γH2AX, MRE11, and NBS1 (7–9). Additionally, the HPV E2 protein and cellular Brd4 proteins associate with and nucleate the formation of viral foci near common fragile sites of the host genome (10). Independently, the E7 protein activates the ATR and ATM signaling pathways both directly (5, 11, 12) and indirectly by inducing cellular proliferation that results in nucleotide deficiency and replication stress (13, 14). All papillomaviruses encode a fusion protein, E8^E2, that restricts viral genome replication and transcription (15, 16). HPV16 E8 mutant genomes overreplicate in undifferentiated cells and express increased levels of viral transcripts and late proteins in differentiated cells compared to the wild-type virus (15, 16). The E8^E2 protein competitively binds to E2BS (E2 binding sites) in the viral genome and interacts with the host corepressor SMRT/NCoR complexes to regulate viral replication and transcription (16, 17).

The HPV genome is associated with cellular histones in both infected cells and in virion particles (18–20). Histones are posttranslationally modified by acetylation, phosphorylation, methylation, sumoylation, and ubiquitination, and these modifications affect chromatin accessibility and impact cellular and HPV gene expression (21, 22). In addition, variants of the canonical histones are associated with different cellular processes, but it is not known whether they also bind to the HPV genome and influence the viral life cycle. One such variant is macroH2A; macroH2A1 is a variant of the canonical H2A histone with a unique C-terminal 30-kDa macro domain. The macroH2A1-encoding gene *H2AFY* encodes two splice variants, macroH2A1.1 and macroH2A1.2, which differ in only 30 amino acids in the carboxyl-terminal macro domain. This results in the formation of a poly-ADP-ribose (PAR) binding pocket in macroH2A1.1, but not in macroH2A1.2 (23). macroH2A1.1 is predominantly expressed in differentiated cells, while macroH2A1.2 is ubiquitously expressed in both differentiated and proliferating cells (24, 25). Both macroH2A1.1 and macroH2A1.2 isoforms are recruited to sites of DNA damage and are involved in either nonhomologous end joining (NHEJ) and/or homologous recombination (HR) (23, 26). macroH2A1.2 also accumulates at common fragile sites upon replication stress (27).

Here, we examine the role of macroH2A1 on HPV genome amplification and transcription during the productive phase of the viral life cycle and show that macroH2A1 associates with HPV replication factories (foci). Depletion of macroH2A1 by small interfering RNA (siRNA) did not affect viral replication but decreased levels of viral transcripts. We show that components of the cellular transcriptional machinery (including RNA Pol II Ser 5, RNA Pol II Ser 2, and Brd4) are present predominantly at the periphery of the replication foci. However, when macroH2A1 is absent from the replication foci, the cellular transcriptional machinery is localized to the interior of the foci, suggesting a role for macroH2A1 in the spatial separation of viral replication and transcription processes during the HPV productive viral life cycle.

RESULTS

macroH2A1 associates with HPV18 and HPV31 viral replication foci. During a preliminary screen to determine whether histones with specific modifications were increased in the chromatin of HPV replication foci, we noted that the variant histone macroH2A1 was highly enriched at HPV31 replication foci in differentiated CIN-612 9E

cells (designated 9E from here on). 9E cells are derived from a CINI cervical lesion and contain extrachromosomal HPV31 genomes that can amplify to high copy number in nuclear foci in differentiated cells (4). Both 9E cells and an HPV negative keratinocyte cell line (NIKS) were cultured on glass coverslips until confluent and differentiated in high-calcium medium for 5 days. Differentiation of these cells results in amplification of viral DNA inside nuclear replication foci. As shown in Fig. 1A and B, viral replication foci (identified by replication protein A, RPA, single-strand DNA binding protein staining) were highly enriched for macroH2A1.2 in 9E cells compared to the rest of the nuclei. We observed macroH2A1.2 enrichment in ~95% of replication foci, and this was irrespective of their size. In contrast, macroH2A1.2 was generally diffuse in control NIKS cells.

The splice variant macroH2A1.1 was also enriched at viral replication factories in 9E cells (Fig. S1A). In contrast, there was no enrichment of the core histones H2A, H3, or H4 in replication foci compared to the rest of the nucleus, showing that this was not simply due to a general increased nucleosomal density (Fig. S1B and C). This does not imply that the HPV genomes are not assembled in canonical histones, but that these histones are not enriched in foci.

Our studies rely heavily on the specificity of the macroH2A1.1 and 1.2 antibodies. Therefore, the expression of macroH2A1.1 and 1.2 was downregulated with siRNA in 9E cells, followed by immunofluorescence and Western blotting with the macroH2A1.1 and 1.2 antibodies (Fig. S2). This confirmed that the macroH2A1.1 and 1.2 antibodies were specific and did not cross-react with viral or cellular proteins. Both macroH2A1.1 (rabbit) and 1.2 (mouse) antibodies were used in subsequent experiments, and this was dependent on the host species of antibodies used to detect other antigens.

To verify that the RPA foci observed in 9E cells were, in fact, HPV replication factories, we confirmed the association of macroH2A1 with the viral genome using immunofluorescent staining for macroH2A1.2 followed by fluorescence *in situ* hybridization (FISH) for the HPV31 genome. Similar to the data shown in Fig. 1A, we observed that ~85% of HPV31 DNA-positive replication foci colocalized with macroH2A1.2 (Fig. 1C to E). High-resolution confocal imaging and 3D image reconstruction showed that macroH2A1 localized in a diffuse pattern throughout most of the foci compared to the punctate pattern of RPA (Fig. 1F and G). To confirm the replication status of the foci, we also stained 9E cells with antibodies against proliferating cell nuclear antigen (PCNA) and observed that ~95% of RPA-positive foci contained PCNA (Fig. S1D). We also examined macroH2A1.2 enrichment at replication factories in a NIKS cell line containing extrachromosomal HPV18 genomes and verified that ~98% of replication foci showed enrichment of macroH2A1.2 (Fig. 2A and B) compared to the rest of the nuclei.

The association of macroH2A1 at replication foci does not correlate with the presence of repressive histone modifications. macroH2A1.2 is often associated with chromatin containing the repressive histone modifications H3K9me2/3 and H3K27me3 (25, 26, 28). Therefore, we examined the localization of these modified histones in differentiated 9E cells and found that, unlike macroH2A1, these modifications were not enriched at viral replication foci (Fig. S3). Together, these findings indicate that the macroH2A1 proteins accumulate at viral replication foci, but this enrichment does not correlate with H3K9me2/3- and H3K27me3-associated repressive chromatin.

Binding of macroH2A1.2 to viral chromatin increases in differentiated cells. Next, to determine whether macroH2A1.2 is incorporated into viral chromatin in replication foci, we performed chromatin immunoprecipitation sequencing (ChIPseq) on growing and differentiated CIN612-9E cells using antibodies against macroH2A1.2. Alignment of the paired-end reads to the HPV31 genome showed binding of macroH2A1.2 across the viral genome, with most binding observed at the 3' end of the late region and the 5' end of the upstream regulatory region (URR) (Fig. 3, upper panel) in both growing and differentiated cells. The relative binding of macroH2A1.2 to the viral genome increased in differentiated conditions relative to the growing conditions (Fig. 3, upper panel). To confirm this, we calculated the binding of macroH2A1.2 to the viral genome using quantitative PCR (qPCR). Primer pairs were designed to amplify different regions
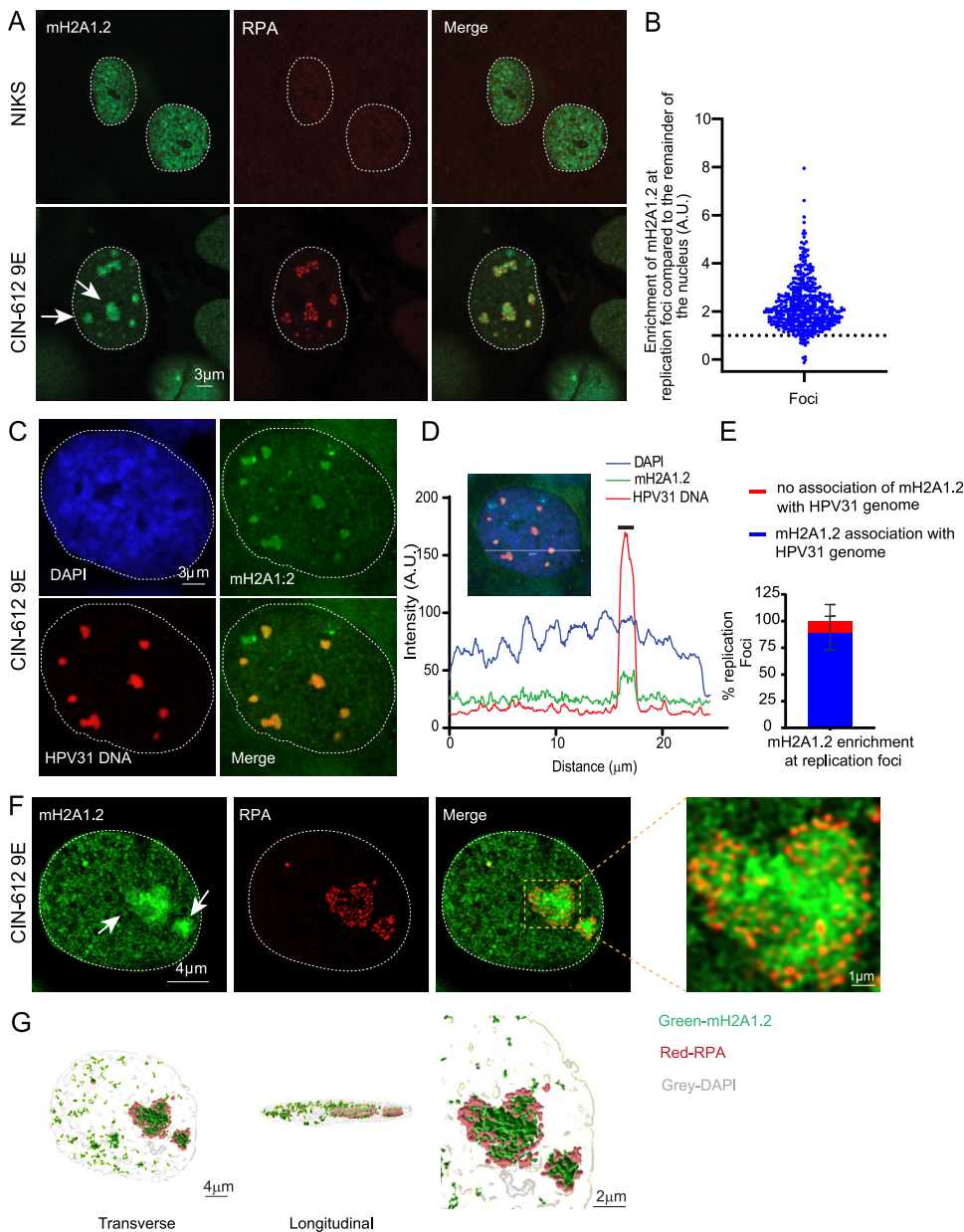
FIG 1 macroH2A1.2 localizes to HPV31 replication foci in 9E cells. (A) Differentiated NIKS or 9E cells were immunostained with antibodies against macroH2A1.2 (green) and RPA (red), and nuclei were counterstained with DAPI (outlined with dotted line). (B) The mean fluorescent intensity of macroH2A1.2 at the foci was calculated using ImageJ (values of >1.0 indicate enrichment). In 9E cells (n = 67), 424/443 RPA-positive foci (~95%) showed enrichment of macroH2A1.2 in three independent experiments. No RPA foci were observed in NIKS cells (n = 213). White arrows indicate different-sized foci. A.U., arbitrary unit. (C) Differentiated 9E cells were analyzed by combined IF-FISH for colocalization of macroH2A1.2 (green) and HPV31 DNA (red). Nuclei were stained with DAPI. (D) Fluorescence intensity line scan obtained by drawing a line through the nucleus shown in panel B using Leica LAS X software. A gray bar above the scan delineates the position of the replication focus. (E) The percentage of replication foci detected by HPV31 DNA FISH with macroH2A1.2 enrichment. A total of 35 cells counted (n = 35) and 172 HPV31-positive foci were scored in two independent experiments. (F) High-resolution image of a deconvolved image is shown from a single slice of Z stacks collected throughout the nucleus. White arrows indicate different-sized foci. The magnified image in the box area demonstrates macroH2A1.2 association with RPA at viral foci. (G) 3D reconstruction of RPA (red) and macroH2A1.2 (green) staining inside a replication factory. Surface-rendering was generated in Imaris from a Z-stack image collected at optimum X, Y, and Z settings and deconvolved in Huygens.

across the HPV31 genome as shown in Fig. 3. Chromatin was prepared from growing and differentiated conditions, and ChIP was carried out with macroH2A1.2, histone H3, and IgG antibodies. In support of the ChIP-PCR data, binding of macroH2A1.2 was observed to all regions of the HPV31 genome and with increased peaks under
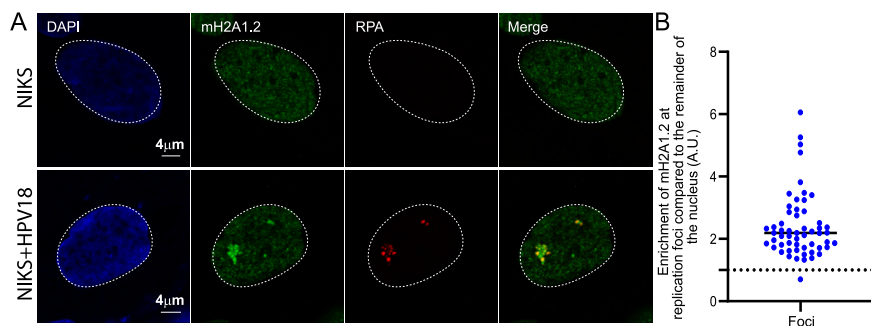
FIG 2 macroH2A1.2 localizes to HPV18 replication foci. (A) Differentiated NIKS or NIKS containing extrachromosomal HPV18 genomes (NIKS-HPV18) were immunostained with antibodies against macroH2A1.2 (green) and RPA (red), and nuclei were stained with DAPI (blue) in two independent experiments. (B) The mean fluorescent intensity of macroH2A1.2 at the foci was calculated using ImageJ (values of >1.0 indicate enrichment). In NIKS-HPV18 cells ($n = 41$), 98% (55/56) of RPA-positive foci showed enrichment of macroH2A1.2. In NIKS, 0/65 cells contained RPA-positive replication foci.

differentiated conditions. Specifically, upon differentiation, macroH2A1.2 binding per viral genome increased 5.2, 5.3, 7.0, 9.3, 10.4, and 3.9-fold at URR1, URR2, early promoter, early and late region, and L1, respectively (Fig. 3).

We have previously shown that bromodomain-containing protein 4 (Brd4) is recruited to HPV viral replication factories (29). Brd4 is a chromatin adaptor protein that binds acetylated lysine residues on histone tails and plays an important role in transcription (30, 31). Brd4 acts as a scaffold for the assembly of large protein complexes on hyper-acetylated promoters and enhancers to promote RNA polymerase II activity to mediate transcription initiation and elongation. For comparison, we carried out ChIPseq to determine the recruitment of Brd4 to the viral genome in growing and differentiated 9E cells. Similar to macroH2A1.2 binding, Brd4 recruitment was increased in differentiated cells compared to cells cultured in proliferative conditions (Fig. 3, lower panel). As expected, the transcription modulator Brd4 was enriched primarily at the early enhancer/promoter region of the viral genome.

macroH2A1 depletion does not affect viral genome amplification in differentiated cells. To analyze the role of macroH2A1 on HPV31 genome amplification, we downregulated both isoforms of macroH2A1 in 9E cells using siRNA and analyzed the viral DNA levels by qPCR and Southern blotting. Cells were transfected with control (Ctrl) siRNA or siRNA against macroH2A1, and total cell DNA was isolated at $T = 0$ days (growing cells) and at $T = 8$ days (differentiated cells) as shown in the scheme in Fig. 4A. To induce differentiation, cells were grown to confluences and then treated with medium containing 1.5 mM calcium at the time indicated. The efficiency of macroH2A1 downregulation was determined by Western blotting (Fig. S2). There was no change in viral copy number in differentiated cells in the macroH2A1-depleted samples compared to control cells (Fig. 4B). Viral genome amplification was also measured by Southern blotting in siCtrl and simacroH2A1 transfected cells. Similar to the data shown in Fig. 4B, there was no difference in viral amplification between macroH2A1-depleted and control cells (Fig. 4C, left and right panels). There was also no change in the ratio of supercoiled monomeric genomes and higher forms that represent multimeric genomes and/or replication intermediates. Taken together, these data show that the absence of macroH2A1 does not affect HPV31 DNA replication or genome copy number.

Depletion of macroH2A1 reduces levels of viral transcripts in differentiated cells. 9E cells can be used to study the different stages of the viral life cycle, as late viral transcription can be activated by cellular differentiation (32). To determine the role of macroH2A1 in viral transcription, we analyzed early, intermediate, and late HPV31 viral transcripts after depletion of macroH2A1 by siRNA. Ctrl siRNA or siRNA against macroH2A1 were transfected into CIN612-9E cells 24 h after plating. For the early stages of the viral life cycle, cells were collected under growing conditions, 48 h after
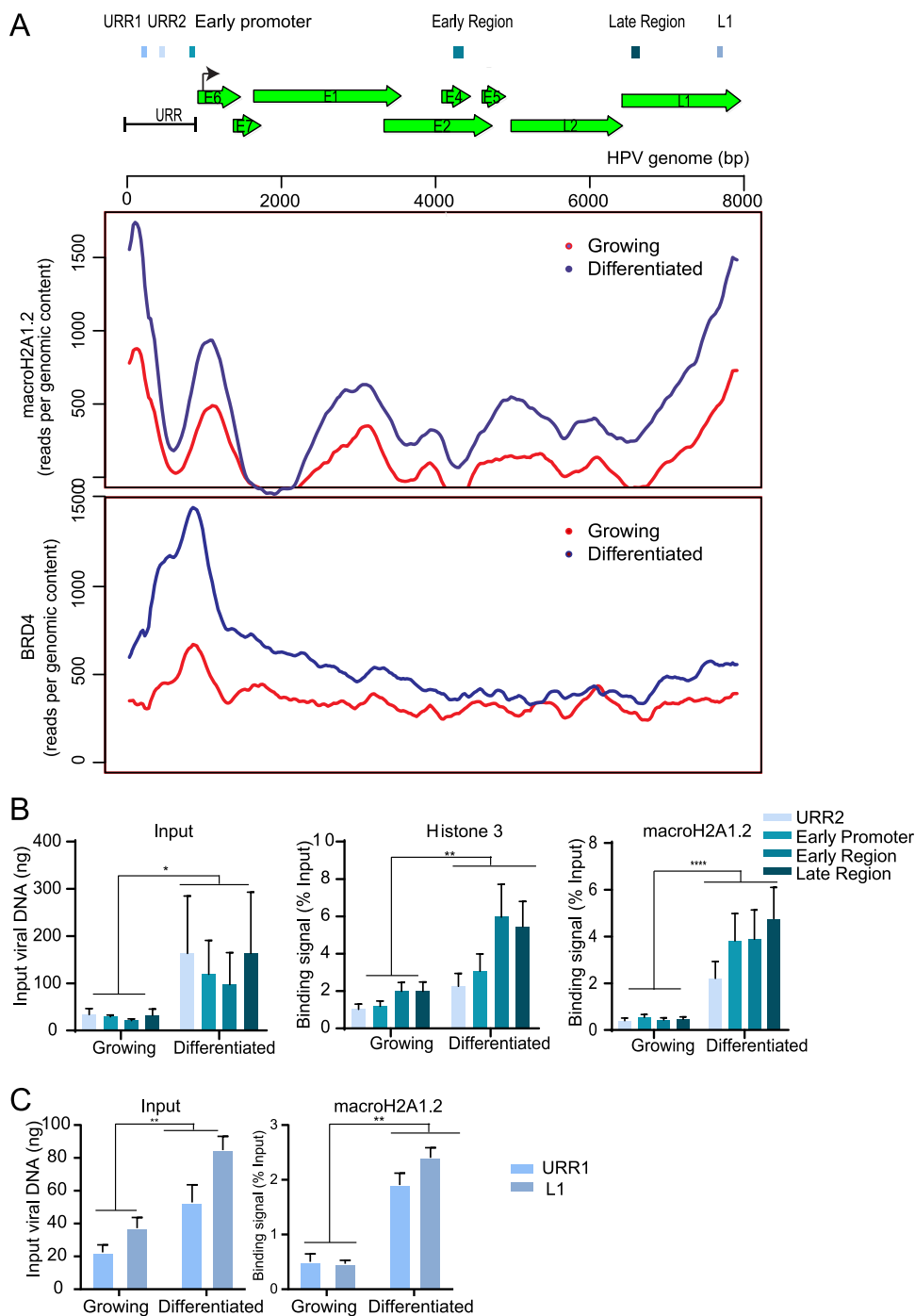
FIG 3 macroH2A1 and Brd4 binding to the HPV31 genome is increased in differentiated conditions. (A) Schematic of a linearized HPV31 genome. URR, upstream regulatory region. ChIPseq was performed with macroH2A1.2 and Brd4 antibodies. Alignment of ChIPseq reads to the HPV31 reference genome in samples from growing and differentiated 9E cells is shown. ChIPseq reads were aligned and analyzed. Data were averaged from two biological replicates. (B) ChIP signals for histone H3 and macroH2A1.2 were expressed as a percentage of immunoprecipitated viral DNA relative to the total amount of input chromatin. Background signal (measured by immunoprecipitating viral DNA with IgG antibody) was subtracted from the corresponding ChIP signals. Binding levels were averaged from three independent experiments. Error bars represent ± standard error of the mean (SEM), and statistical significance was calculated using a paired Student's t test. (C) ChIP signals were expressed as a percentage of immunoprecipitated viral DNA relative to the total amount of input chromatin. Background signal (measured by immunoprecipitating viral DNA with IgG antibody) was subtracted from the corresponding ChIP signals. URR1 and L1 regions were selected from ChIPseq peaks, and ChIP was carried out independent of the ChIP experiment shown in panel B. Binding levels were averaged from two independent experiments. Error bars represent ± standard deviation (SD), and statistical significance was calculated using a paired Student's t test. *, $P < 0.05$; **, $P < 0.005$; ***, $P < 0.005$.
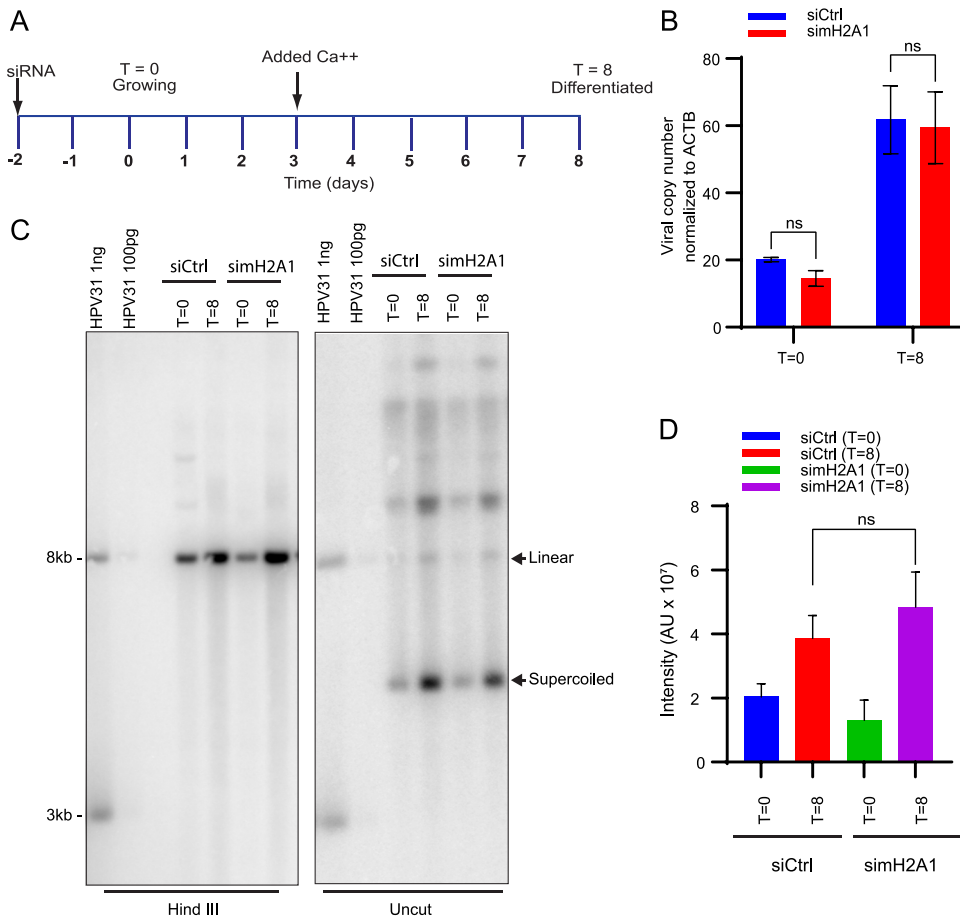
FIG 4 macroH2A1 does not regulate levels of viral replication of HPV31 genomes in CIN612-9E cells. (A) Timeline. Cells were transfected with either Ctrl or macroH2A1 siRNA 24 h after plating. Two days later, DNA was extracted at $T = 0$ days for growing or $T = 8$ days for differentiated conditions as indicated in the diagram. A Western blot showing the efficiency of downregulation is shown in Fig. S2. (B) The viral copy number was measured by qPCR after macroH2A1 siRNA treatment. (C) Southern blot analysis of DNA extracted from the siCtrl and simacroH2A1 samples after macroH2A1 depletion. The arrows indicate linear and supercoiled viral genomes. The blot is representative of two independent experiments. (D) Quantification of the linear HPV DNA from the Southern blot. Statistical significance was determined using a paired t test for changes in HPV replication. ns, not statistically significant. For panels B and D, errors bars represent ± SEM from four and two independent experiments, respectively.

transfection ($T = 0$). For later stages of the viral life cycle, cells were differentiated in calcium-containing medium as indicated in the time line in Fig. 5A. mRNA expression levels of the macroH2A1 isoforms and viral transcripts including E6*I (early), E1^E4 (intermediate), and L1 spliced (late) were measured by qRT-PCR (Fig. 5B and C). Both splice variants, macroH2A1.1 and macroH2A1.2, were significantly downregulated (~95%) under growing ($T = 0$) and differentiated conditions ($T = 8$) (Fig. 5B). Depletion of macroH2A1 resulted in no significant change in expression levels of early (E6*I) transcripts. However, mRNA expression levels of both intermediate (E1^E4) and late transcripts (L1 spliced) were significantly reduced in differentiated cells upon depletion of macroH2A1 (Fig. 5C).

HPV late gene expression is regulated by the keratinocyte differentiation process, so we monitored this by measuring the mRNA levels of the keratinocyte differentiation induced genes, involucrin and filaggrin (Fig. 5D). macroH2A1 depletion decreased mRNA expression levels of both transcripts in the differentiated cells, making it difficult to conclude whether viral transcription was directly regulated by macroH2A1 or whether the reduction in viral transcription was indirect and the result of impaired differentiation. Creppe et al. have shown that macroH2A1 expression increases in the
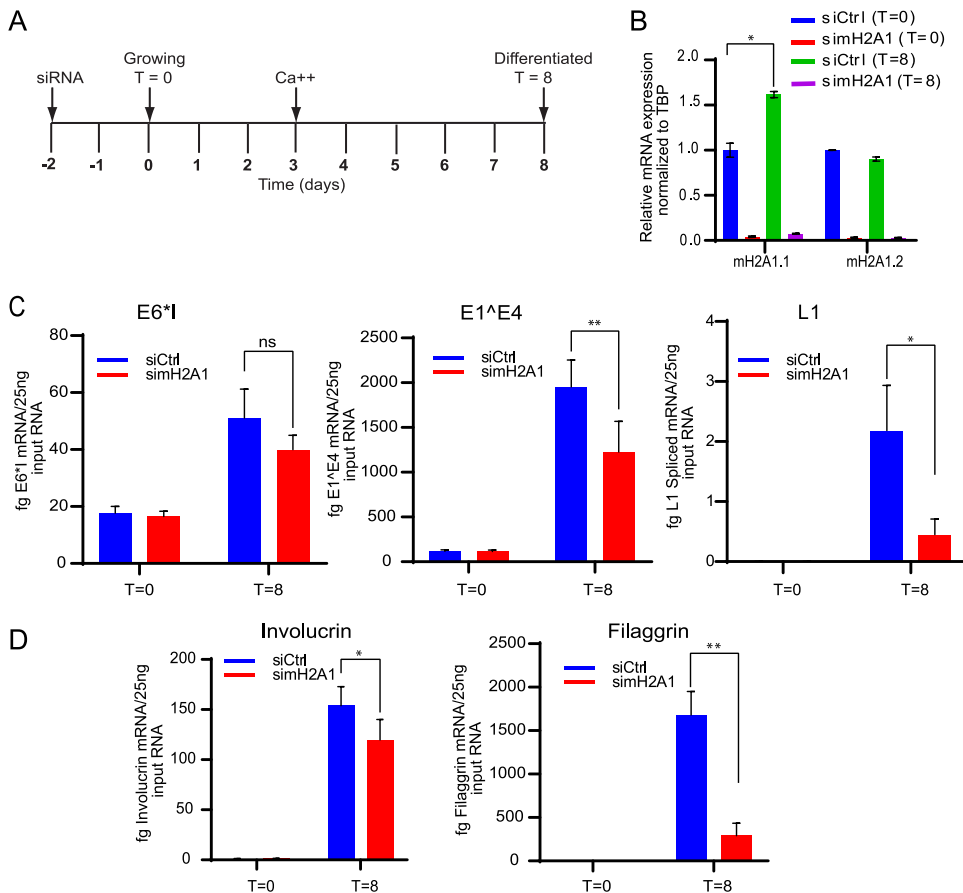
FIG 5 Depletion of macroH2A1 reduces the levels of HPV viral transcripts. (A) Timeline; 9E cells were transfected with either Ctrl or macroH2A1 siRNA 24 h after plating. Two days later, RNA was extracted at $T = 0$ days for growing or $T = 8$ days for differentiated conditions as indicated in the timeline. (B) The efficiency of depletion was monitored by measuring levels of macroH2A1.1 and macroH2A1.2 transcripts (C) Viral transcripts E6*I, E1^E4, and spliced L1 were detected by qRT-PCR (D) Transcripts for the keratinocyte differentiation markers, involucrin and filaggrin, were measured by qRT-PCR, as indicated. All results were obtained from four independent experiments. A paired Student's t test was used to determine statistical significance. Errors bars represent $\pm$ SEM; *, $P < 0.05$; **, $P < 0.005$; ns, not statistically significant.

differentiated layers of skin and that depletion of macroH2A1 in human keratinocytes interferes with activation of differentiation genes and the formation of stem cell holoclones (33). We did observe a small increase in macroH2A1 RNA and protein in our calcium-differentiated 9E cells (Fig. 5B and Fig. S2B), and downregulation of macroH2A1 did reduce RNA levels of involucrin and filaggrin. In summary, our data show that depletion of macroH2A1 reduces HPV31 late gene expression; however, this could be indirect due to effects on keratinocyte differentiation.

macroH2A1 is not enriched in HPV16 E8^E2 mutant replication foci. Productive replication and transcription of HPV viral genomes is inhibited by the viral E8^E2 repressor protein (16). HPV16 genomes mutated to eliminate expression of E8^E2 have increased viral DNA replication and transcription, even in the absence of keratinocyte differentiation (34). In our laboratory, we find that keratinocyte cell lines containing an HPV16 genome mutated in E8^E2 (HPV16ΔE8^E2) form large replication foci in the absence of keratinocyte differentiation (manuscript in preparation). Therefore, we used cell lines containing wild-type HPV16 and HPV16ΔE8^E2 genomes to analyze the location of macroH2A1 in these replication foci. HPV16 wild-type cells contained only a few, small replication foci. However, in cells containing the HPV16ΔE8^E2 genome, multiple small and large foci were present in the nucleus of many cells (Fig. 6A and B). Foci formed with HPV16ΔE8^E2 showed two phenotypes. In ~77% of foci macroH2A1.2 was
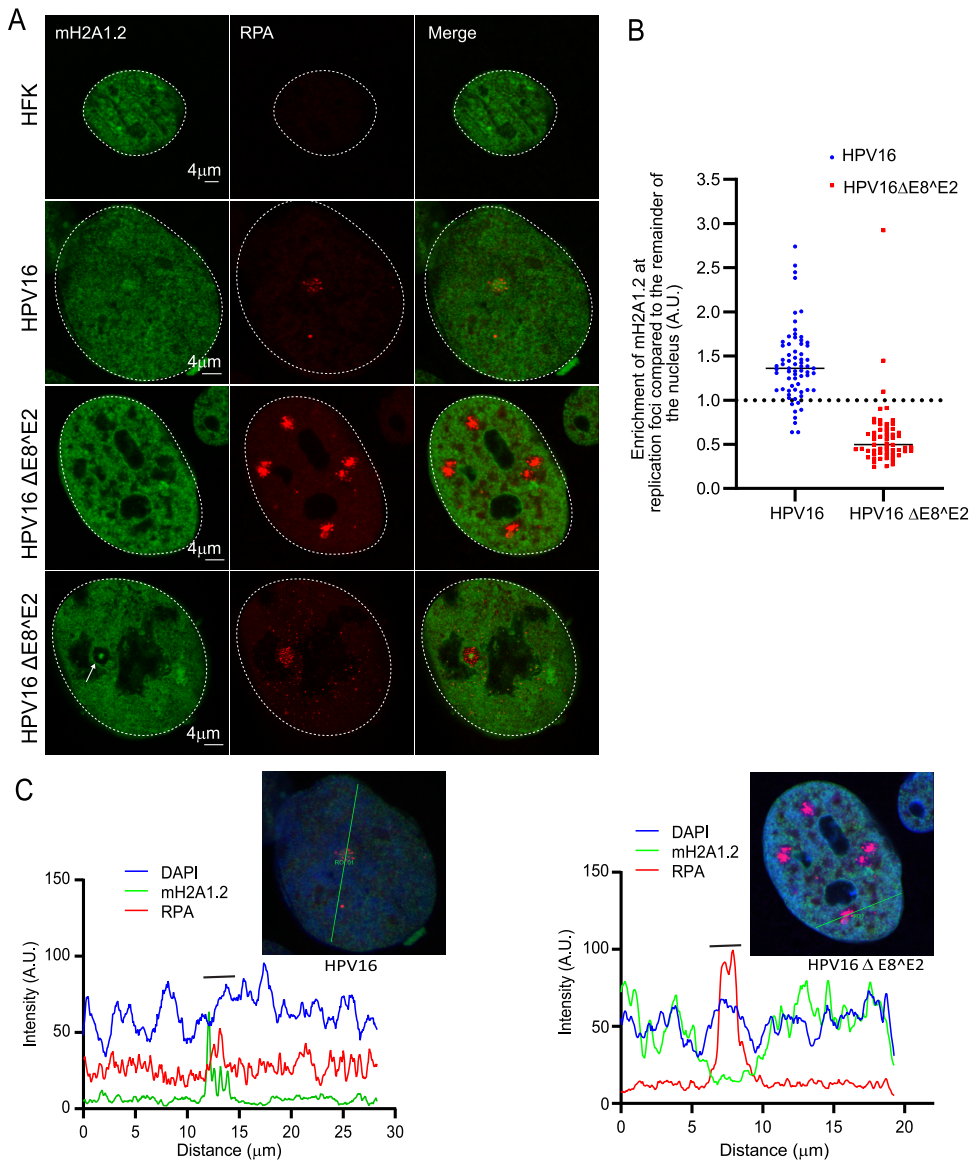
FIG 6 macroH2A1 is not recruited to the replication in HPV16ΔE8^E2 cells. (A) HFK (strain 20) cell lines containing either the HPV16 wild-type or HPV16ΔE8^E2 genome were immunostained with antibodies against macroH2A1.2 (green) and RPA (red). Nuclei are indicated with dotted lines. A white arrow indicates core staining of macroH2A1.2. (B) Quantification of panel A. The mean fluorescent intensity of macroH2A1.2 was calculated using ImageJ (values of >1.0 indicate enrichment). A total of 136 cells were scored with the parental HFK20 strain as a negative control (no RPA foci were detected). In HPV16ΔE8^E2 cells, 58 RPA-positive foci were counted from 41 cells (n = 41) in two independent experiments. A total of 94.8% of foci (55/58) showed no enrichment of macroH2A1. In wild-type HPV16 genome-containing cells (n = 66), 68 RPA-positive foci were scored and 89.1% (61/68) showed enrichment of macroH2A1 (mostly single foci are present in wild-type HPV16 cells). (C) Fluorescence intensity light scans obtained by drawing a line through a nucleus shown in panel A. A gray bar above the scan delineates the position of the replication focus.

mostly absent; in ~23% of the foci a small amount of macroH2A1.2 was present as an intensely stained central core (Fig. 6A). This showed that macroH2A1.2 was enriched in the small wild-type foci but was mostly depleted from the majority of replication foci in HPV16ΔE8^E2 mutant cells (Fig. 6B), irrespective of the size. To ensure that the HPV16ΔE8^E2 replication foci were not simply depleted of all histones, the presence of H2A, H2B, H3, and H4 was analyzed by immunofluorescence in HPV16ΔE8^E2 replication foci. The canonical histones were neither depleted nor enriched in the HPV16ΔE8^E2 replication foci (Fig. S4).

macroH2A1 is incorporated in viral replication foci independent from DNA damage. macroH2A1.2 is known to mediate a dynamic transition of chromatin from a relaxed accessible state to a condensed inaccessible state at double-strand DNA breaks (DSBs) (26). The accumulation of macroH2A1.2 in this compact chromatin environment is ATM-dependent and promotes the retention of the homologous recombination protein BRCA1 at the DSBs. HPV recruits several repair factors from ATM and ATR signaling pathways to replication foci (5, 29, 35), and the enrichment of HR factors indicates that amplification of viral genomes during productive infection might involve recombination-directed replication (5, 11, 12, 36). Therefore, we asked whether macroH2A1 enrichment at viral replication foci correlated with DNA damage signaling. We investigated the localization of mH2A1 along with DNA damage markers γH2AX, 53BP1, BRCA1, and RAD51 in the HPV16 wild-type and HPV16ΔE8^E2 mutant cell lines. γH2AX was present in 100% of HPV16 wild-type and HPV16ΔE8^E2 replication foci, indicating that DNA damage response (DDR) signaling pathways were intact in HPV16 wild-type and HPV16ΔE8^E2 mutant cells (Fig. 7A and B). However, despite active DDR signaling in the foci in E8^E2 mutant cell lines, macroH2A1.1 was depleted in ~94% of these foci. BRCA1, RAD51, and 53BP1 were also enriched at 100% of viral replication foci in both HPV16 wild-type and HPV16ΔE8^E2 mutant cells. Altogether, these data show that the enrichment of macroH2A1 at viral replication foci does not correlate with DNA damage signaling.

Cellular RNA transcriptional machinery localizes outside viral replication foci. It has been shown previously that the presence of macroH2A in chromatin inhibits transcription by interfering with transcription factor binding and SWI/SNF (switch/sucrose nonfermentable) remodeling (37), which correlates with repressive H3K9me3 and H3K27me3 marks. Although macroH2A1 is predominantly found in repressed chromatin, it can also activate expression of a subset of genes (25). Specifically, macroH2A1 is a positive regulator of a subset of the genes that contain macroH2A1 in the transcribed region. RNA polymerase II (RNA Pol II)-mediated transcription, from initiation to termination, is a highly complex process (38). The C-terminal domain (CTD) of RNA Pol II contains heptad repeats that become phosphorylated at serine position 5 (Ser 5) and serine position 2 (Ser 2) during transcription initiation and elongation, respectively (38). To date, nothing is known about the intranuclear location of HPV transcription with respect to replication foci at late stages of infection. Therefore, we examined the location of RNA Pol II in 9E cells to determine whether it correlated with the enrichment of macroH2A1 at the HPV31 replication foci.

As shown in Fig. 8A and B, RNA Pol II phosphorylated on serine 2 was observed in two different locations with respect to the replication foci; it was either reduced or absent from the interior of the viral replication foci compared to the rest of the nucleus (~73% of foci) or was present at the periphery in a satellite pattern in a fraction of the foci (~18% of foci). The remainder of the foci (9%) did not show any exclusion of RNA Pol II Ser 2. Figure 8A shows a high-resolution confocal image for RNA Pol II Ser 2 on the surface of the viral replication foci. The Pearson's coefficient obtained from colocalization analysis confirmed that the localization of macroH2A1.2 and RNA Pol II Ser 2 were mutually exclusive at the replication foci (Fig. 8C). Similar to RNA Pol II Ser 2, RNA Pol II Ser 5 was detected in a satellite localization in ~24% of replication foci and was reduced or absent inside ~64% of foci (Fig. S5). The remaining 12% of foci did not show any exclusion of RNA Pol II Ser 5.

Notably, the transcription factor Brd4 also localizes in a satellite pattern around the foci in 9E cells (29). Further analysis showed that Brd4 and RNA Pol II Ser 5 colocalized in the satellite pattern on the periphery of viral replication foci, and this was confirmed by high-resolution confocal imaging (Fig. 8D and E). The high degree of colocalization was confirmed by colocalization analysis, and the Pearson's coefficient is shown in Fig. 8F. These data suggest that very little viral transcription takes place inside the replication foci, and instead, viral transcription occurs on the surface of those foci displaying an enriched satellite pattern of RNA polymerase and Brd4. Thus, we propose that
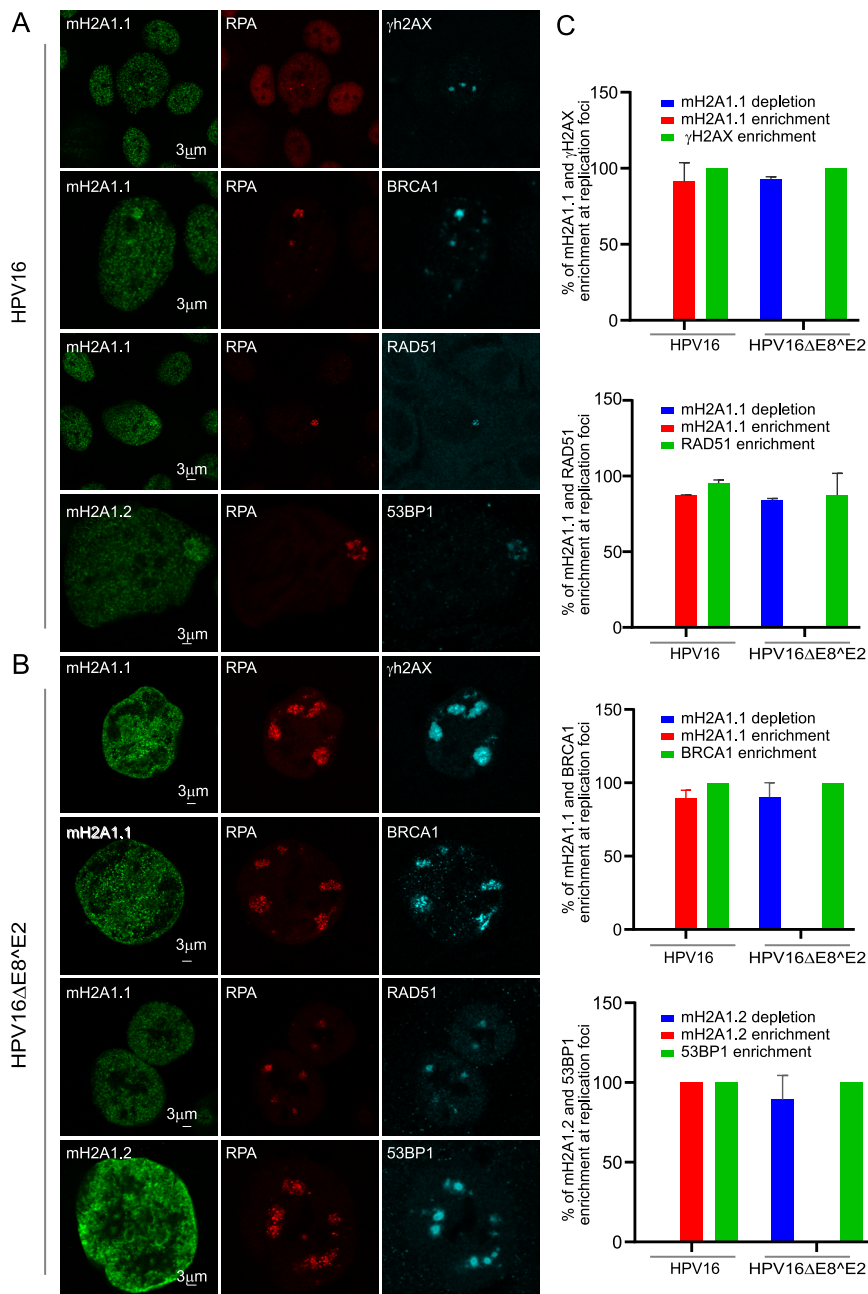
FIG 7 macroH2A1 is recruited to the viral replication foci in a DNA damage-independent manner. (A) HFK39 (39 strain) cell lines containing HPV16 wild-type genomes were immunostained with antibodies against macroH2A1.1 or macroH2A1.2 (green), RPA (red), and DNA damage- and repair-associated proteins (γH2AX, BRCA1, RAD51, and 53BP1, in cyan). (B) HPV16ΔE8^E2-containing cell lines were immunostained with antibodies against macroH2A1.1 or macroH2A1.2 (green), RPA (red), and DNA damage- and repair-associated proteins (γH2AX, BRCA1, RAD51, and 53BP1, in cyan). (C) Quantitation of the experiments shown in panels A and B. For macroH2A1.1 and γH2AX staining, 40 RPA-positive foci were scored from 26 HPV16 wild-type cells and 141 foci in 31 HPV16ΔE8^E2 cells. For macroH2A1.1 and RAD51, 47 foci were scored in 44 HPV16 wild-type cells and 80 foci in 18 HPV16ΔE8^E2 cells. For macroH2A1.2 and 53BP1, 34 foci were scored in 20 HPV16 wild-type cells, and 115 RPA-positive foci were scored in 33 HPV16ΔE8^E2 cells. For macroH2A1.1 and BRCA1, 22 foci in 20 HPV16 wild-type cells and 59 RPA-positive foci in 16 HPV16ΔE8^E2 cells were scored. Quantitation was from two independent experiments.

there is a spatial separation of replication and transcription at the productive stage of the HPV infectious cycle.

RNA transcriptional machinery is localized inside HPV16ΔE8^E2 foci. We hypothesized that macroH2A1 might be localized to the replication foci to prevent
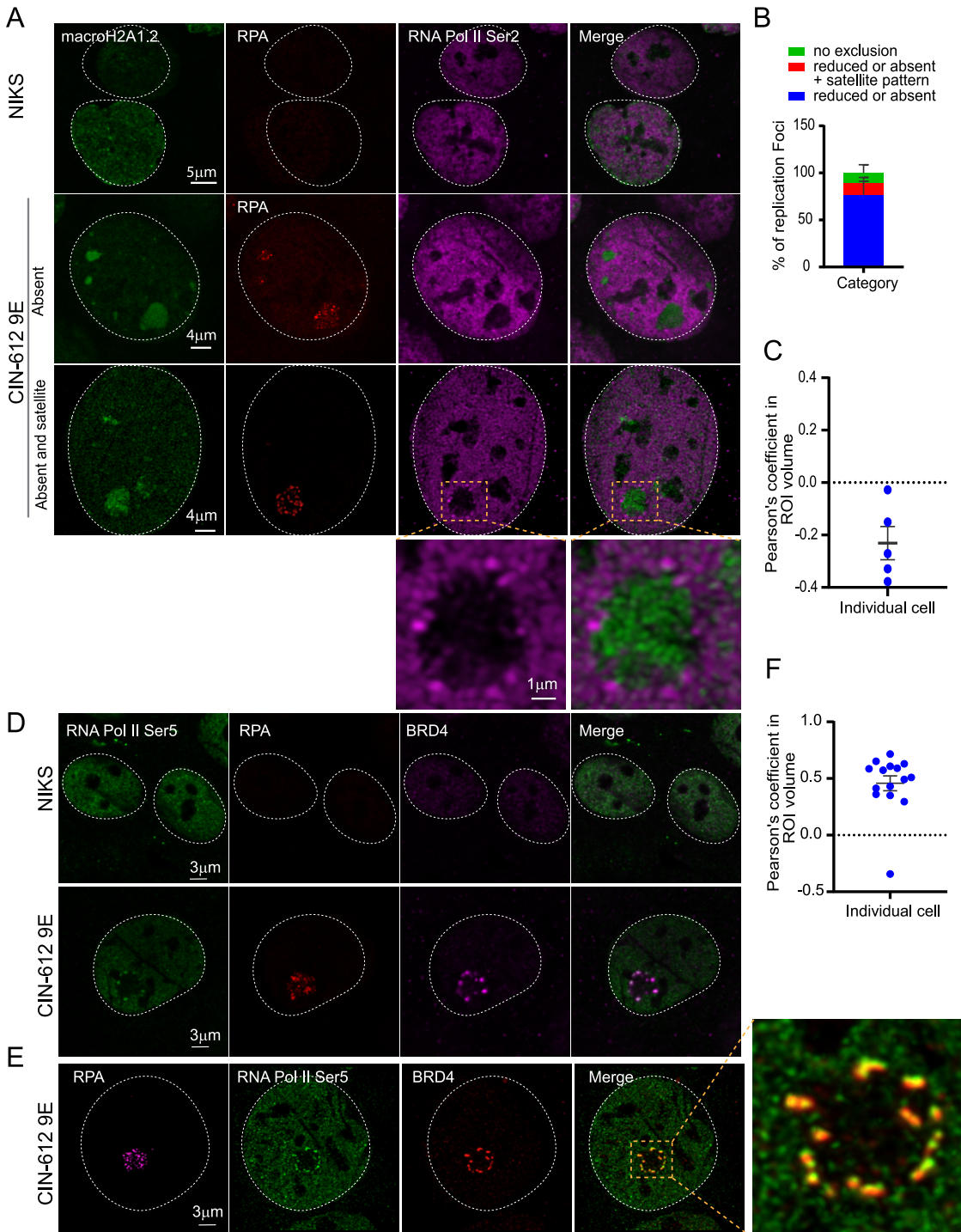
FIG 8 RNA Pol II Ser 2 is located outside the HPV31 replication foci in 9E cells. (A) Differentiated NIKS or 9E cells were immunostained with antibodies against macroH2A1.2 (green), RPA (red), and RNA Pol II Ser 2 (purple). A white dotted line outlines the nuclei. (B) Distribution of RNA Pol II Ser 2 at replication foci by visual counting (n = 55 cells, 130 foci) in two independent experiments. (C) Confocal images (3D) were deconvolved using Huygens Essential. Colocalization analysis was performed in an ROI (region of interest) defined by the RPA signal in Imaris (version 9.6.0). The percentage of ROI macroH2A1.2 and percentage of ROI RNA Pol II Ser 2 colocalized were calculated, and the Pearson's coefficient in the ROI volume was calculated and shown. (D) Cells were immunostained with antibodies against RNA Pol II Ser 5 (green), RPA (red), Brd4 (CW152—recognizes both Brd4S and Brd4L; purple). In differentiated CIN-612 9E cells, 233 foci in 71 cells (n = 71) were counted using RPA as a marker for viral replication foci. A total of 34 cells were scored for differentiated NIKS as a negative control. A white dotted line marks the nuclei. (E) A high-resolution image generated from deconvolved Z stacks collected throughout the nucleus. A single slice is shown, representing the colocalization of Brd4 and RNA Pol II Ser 5 at the periphery of a viral replication foci. The magnified box demonstrates Pol II Ser 5 and Brd4 localization at viral foci. (F) Confocal images

transcription of replicating DNA, thereby restricting transcription to the surface of the foci. To test this, we assessed the location of RNA Pol II in foci generated by HPV16ΔE8^E2 mutant genomes, which do not contain enriched macroH2A1. As shown in Fig. 9, in HPV16 wild-type cells, RNA Pol II Ser 5 is often localized outside the foci (with Brd4), and macroH2A1.2 is enriched throughout the foci, as found for HPV31 foci in 9E cells. In contrast, foci formed with HPV16ΔE8^E2 showed two phenotypes. In ~75% of the foci macroH2A1 was mostly depleted; in ~25% of the foci a small amount of macroH2A1.2 was present as an intensely stained core (Fig. 9A). Furthermore, the location of RNA Pol II Ser 5 and Brd4 correlated inversely with these macroH2A1.2 patterns; when macroH2A1.2 was completely depleted from the foci, Brd4 and RNA pol II Ser 5 were present inside; however, when macroH2A1.2 was present in the core, then Brd4 and RNA Pol II Ser 5 were localized in a ring around the foci (Fig. 9A). In conclusion, these data suggest that the function of macroH2A1.2 is to exclude the transcription machinery at the periphery of the foci.

macroH2A1 prevents the formation of acetylated chromatin within replication foci. Brd4 binds to acetylated chromatin through its tandem bromodomains and promotes transcriptional initiation and elongation by recruiting mediator and pTEFb complexes, respectively (39, 40). We have also previously shown that the chromatin that surrounds HPV31 foci in 9E cells is enriched in acetylated chromatin (29). To determine the relationship between acetylated chromatin (histone H3 K9ac/18ac), Brd4, and macroH2A1 in the replication foci, we analyzed their localization in HPV16 wild-type and HPV16ΔE8^E2 mutant genome-containing cells. In support of this hypothesis, macroH2A1.2 is depleted from most of the HPV16ΔE8^E2 mutant foci (~70% of foci), while histone H3K9ac/K18ac is enriched within the foci (Fig. 9B). Conversely, macroH2A1.2 was enriched at the HPV16 wild-type (WT) foci, but H3K9/18 acetyl was neither depleted nor enriched at these foci (Fig. 9B). Altogether, this suggests that the absence of macroH2A1.2 from the foci allows enhanced levels of formation of active chromatin inside the foci.

The E8^E2 proteins recruit corepressor complexes to viral replication foci. The E8^E2 proteins from HPV1, 8, 16, and 31 interact with the NCoR/SMRT corepressor core complex (GPS2, HDAC3, NCoR, SMRT, and TBl1 proteins) to repress viral transcription and E1/E2-dependent replication (17). Since macroH2A1 was absent from the majority of HPV16ΔE8^E2 foci, we investigated the recruitment of SMRT, along with macroH2A1.2, to HPV31, HPV16 wild-type, and HPV16ΔE8^E2 foci. As shown in Fig. 10A (right panel), macroH2A1.2 and SMRT were present in HPV31 and HPV16 wild-type foci (~91% of foci in 9E cells and ~68% of foci in HPV16 wild-type cells). In contrast, in the HPV16ΔE8^E2 cell line, macroH2A1.2 was depleted from the foci and there was no enrichment of SMRT. Therefore, there is a correlation between the enrichment of both SMRT and macroH2A1 to the foci. However, although both factors are present in the foci, they do not localize exactly to the same regions, making it less likely that this is a direct interaction (Fig. 10A).

HPV16 E2-TA and E8^E2 proteins are recruited to replication foci in HPV16 wild-type and HPV16ΔE8^E2 genome cell lines. Our observations indicate that transcriptional repressor complexes are present throughout wild-type HPV replication foci and transcriptional activity is restricted to the surface. In contrast, foci generated in the absence of E8^E2 are larger, do not recruit corepressor complexes, and contain evidence of transcriptional activity throughout the foci. Dreer et al. have shown that the HPV31 E8^E2 protein localizes to replication foci formed by the E1 and E2 proteins wherein the E8 moiety recruits the corepressor proteins (16). To determine the localization of the HPV16 E2-TA and E8^E2 proteins in the foci, we used two different HPV16 E2 antibodies, one that recognizes the unique N-terminal domain of the E2-TA protein and the other that recognizes the DNA binding domain shared by both E2 proteins.

FIG 8 Legend (Continued)
(3D) were deconvolved using Huygens Essential, and colocalization analysis was performed in the replication foci ROI defined by the RPA signal using Imaris from a total of 15 cells ($n = 15$, foci = 41). The percentage of ROI Brd4 and percentage of ROI Pol II Ser 5 colocalized were calculated, and the Pearson's coefficients in the ROI volumes are shown.
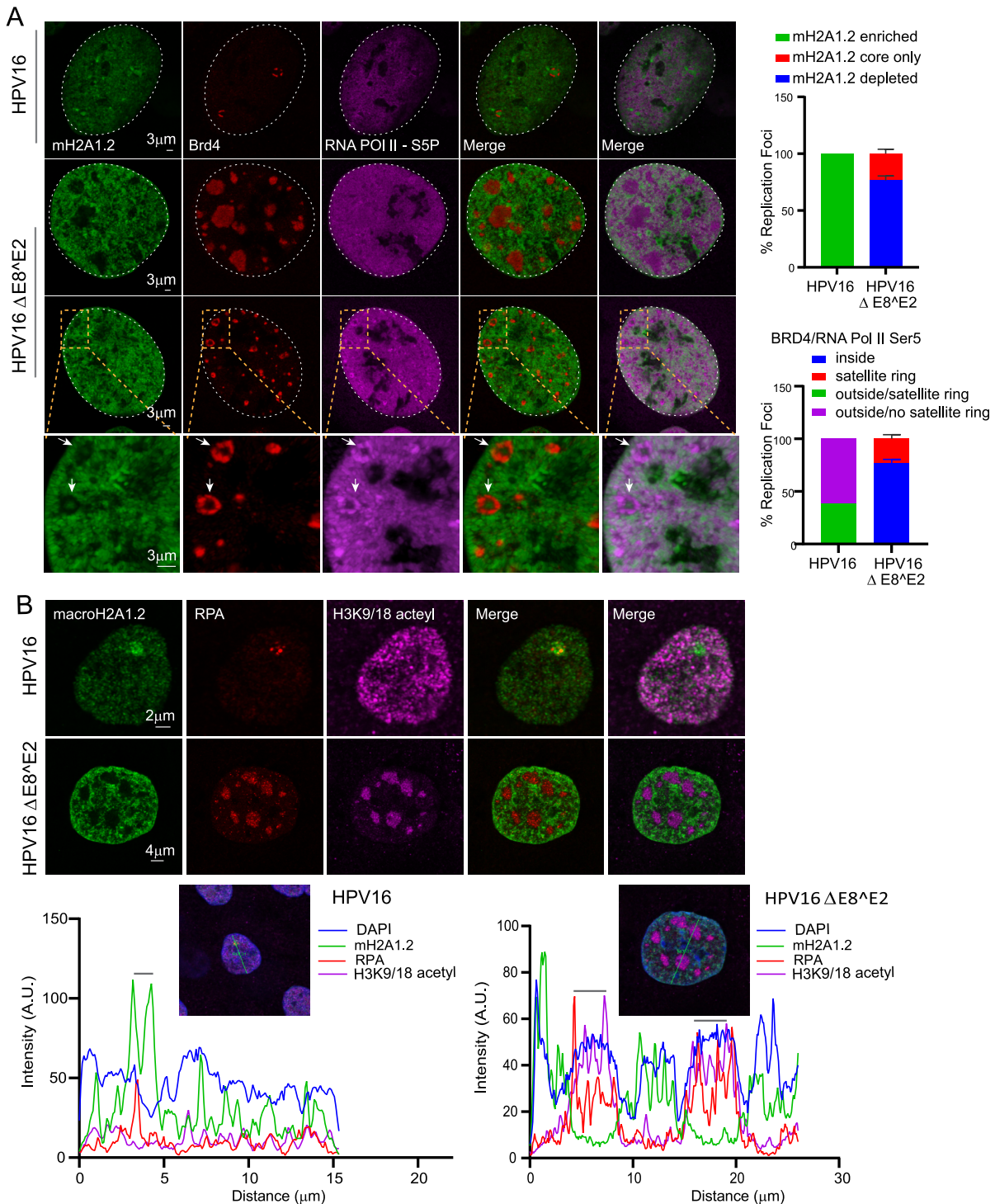
FIG 9 RNA Pol II Ser 5, Brd4, and acetylated histones are localized predominantly inside the replication foci in HPV16 ΔE8^E2 cells. (A) HFK (39 strains) cell lines containing HPV16 wild-type or HPV16ΔE8^E2 genomes were immunostained with antibodies against macroH2A1.2 (green), Brd4 (red), and RNA Pol II Ser 5 (purple). Nuclei were stained with DAPI (indicated by white dotted line). Quantitation from two independent experiments is shown to the right. In the upper graph, in 12 HPV16 wild-type cells, 100% of foci (13/13) showed enrichment of mH2A1.2. In 32 HPV16 ΔE8^E2 cells, 192 RPA-positive foci were scored for either depletion or a small residual amount of macroH2A1.2 at the core. Foci indicated with a white arrow show the core staining of macroH2A1.2. In the lower graph, the locations of RNA Pol II Ser 5 and Brd4 with respect to the foci are shown from HPV16 wild-type cells (13 foci) and HPV16ΔE8^E2 cells (192 foci in 32 cells). Foci were visually counted from two biological experiments. (B) HPV16 wild-type and HPV16 ΔE8^E2 genome-containing cells were immunostained with antibodies against histone H3K9/18 acetyl (purple), macroH2A1.2 (green), and RPA (red). Nuclei were stained with DAPI (not shown), and the distributions of H3K9/18 acetyl in HPV16 wild-type (n = 35, 37 RPA-positive foci) and HPV16ΔE8^E2 cells (n = 44, 188 RPA-positive foci) were analyzed by visual counting. Cells were scored from two biological independent replicates. (Lower panel) Fluorescence intensity scans obtained by drawing a line through a nucleus using Leica LAS X software. A gray bar above the scan delineates the position of the replication focus.
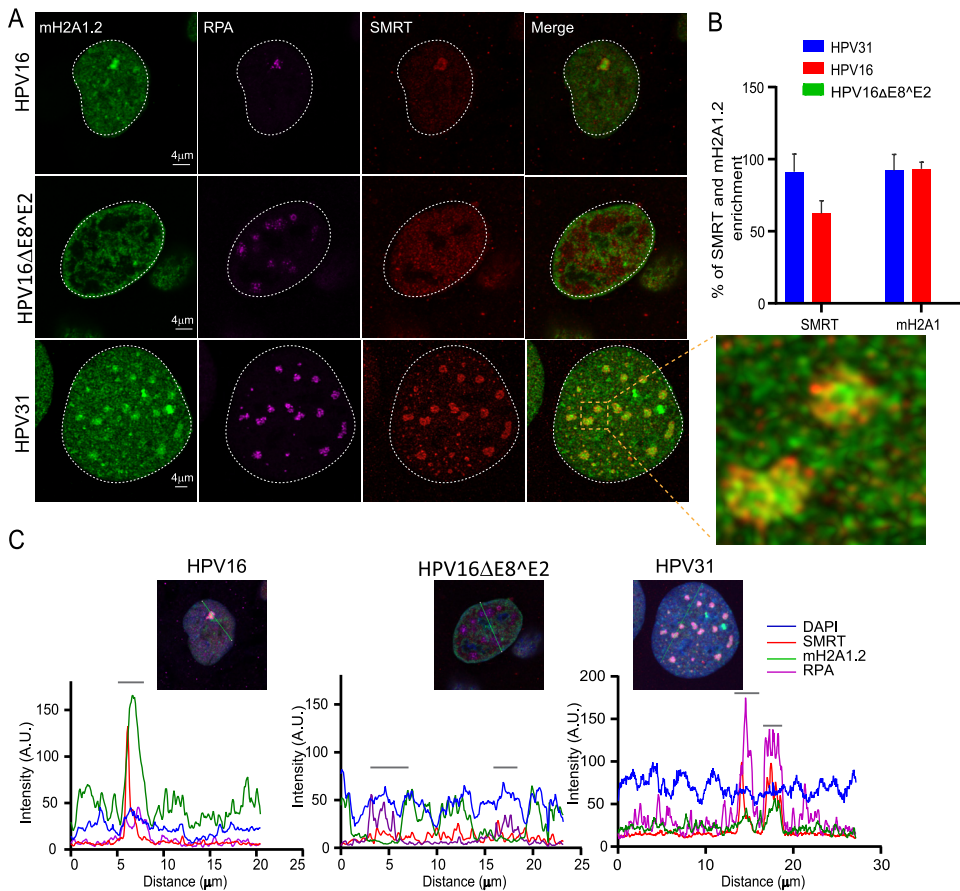
FIG 10 macroH2A1 and SMRT corepressor independently localize to replication foci. (A) HPV31 (9E cells), HPV16 wild-type cells, and HPV16 ΔE8^E2 genome-containing cells were immunostained with antibodies against RPA (purple), macroH2A1.2 (green), and SMRT (red). A white dotted line outlines the nucleus. A high-resolution image of a deconvolved image is shown from a single slice of Z stacks collected throughout the nucleus for the 9E cell. The magnified image in the box area demonstrates macroH2A1.2 and SMRT localization at replication foci. (B) The percentage of foci enriched for SMRT and macroH2A1.2 in differentiated cells containing HPV31 (n = 50 9E cells, RPA-positive foci = 159), HPV16 wild-type (n = 28 cells, RPA-positive foci = 29), and HPV16ΔE8^E2 (n = 53 cells, RPA-positive foci = 241) was analyzed. Data are from two independent biological replicates. (C) Fluorescence intensity scans obtained by drawing a line through the nuclei indicated using Leica LAS X software. A gray bar above the scan delineates the position of the replication focus.

The specificity of these antibodies is shown in Fig. S6. As expected, in foci generated by the HPV16ΔE8^E2 genome, the staining pattern was very similar for both antibodies since only the E2-TA protein was present. Two patterns of E2 staining were observed; E2 was either enriched throughout the foci or present in a satellite ring around the foci similar to localization of Brd4 and RNA Pol II Ser 5 (Fig. 9). This pattern correlated with the macroH2A1 patterns; when macroH2A1.2 was completely depleted from the foci (~85% of foci), E2 was present inside; however, when macroH2A1.2 was present in the core (~15% of foci), then E2 was localized as a ring around the foci (Fig. 11 and Table 1). In HPV16 wild-type cells, there were three patterns observed. Both antibodies either detected E2 proteins in the satellite regions around the foci (~22%) or throughout the foci (~26%). The satellite localization was similar to Brd4 and Pol II Ser 5 localization. However, in most of the cells, only the C-terminal antibody stained throughout the foci (~52% of the foci); we conclude that this is the E8^E2 protein and that it localizes throughout the foci similar to the localization of macroH2A1.2 (Fig. 11 and 12).

Taken together, these studies show that the E8^E2 protein can recruit cellular corepressor proteins to HPV replication foci to repress transcription, while the E2-TA
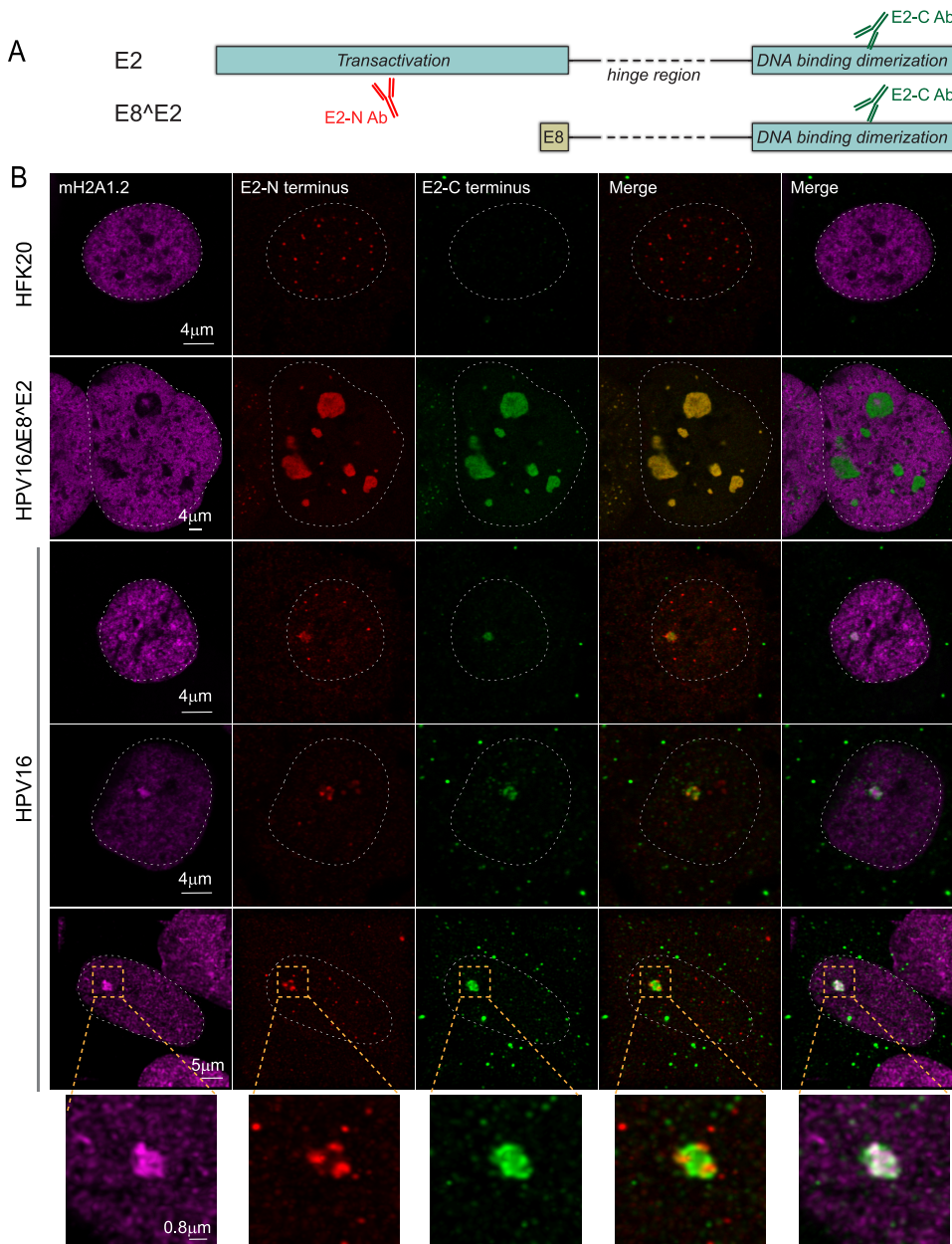
FIG 11 HPV16 E2-TA and E8^E2 proteins are recruited to replication foci in HPV16 wild-type and HPV16ΔE8^E2 genome cell lines. (A) Diagram of the E2-TA and E8^E2 proteins and antibodies. (B) HPV16 wild-type and HPV16ΔE8^E2 genome-containing cells were immunostained with antibodies against macroH2A1.2 (cyan), E2 (N-terminal antibody; red), and E2 (C-terminal antibody; green). A white dotted line outlines the nucleus. The specificities of the E2 antibodies are shown in Table 1 and Fig. S6. In HPV16 wild-type cells, macroH2A1.2 was enriched at ∼100% (37/37) of foci collected from $n = 37$ cells. About 52% of foci (19/37) showed a satellite pattern for E2 N-terminal antibody, while the C-terminal E2 antibody was stained throughout the foci; ∼22% (8/37) of the foci showed a satellite pattern for both the E2 N-terminal and C-terminal staining pattern; in the remaining ∼26% of the foci (10/37), both antibodies were stained throughout the foci. In HPV16ΔE8^E2 genome cell lines, 251 RPA-positive foci were scored from $n = 39$ cells, and ∼85% of foci (214/251) showed enrichment of E2 (both through N-terminal and C-terminal antibody) inside the foci, and ∼15% of the total foci (37/251) showed a ring around the foci for E2 (not shown). Data were obtained by visual counting from two experiments.

protein is located (at least initially) on the surface of the foci, where it colocalizes with Brd4 and RNA Pol II Ser 2/5, implying that these are transcriptionally active complexes. The histone variant macroH2A1 is also recruited to foci in cells that express the HPV E8^E2 protein, and we postulate that both cellular macroH2A1 and viral E8^E2

TABLE 1 Specificities of E2 antibodies[a]

Cells-virus	E2-N Ab (aa 1–201) (detects only E2-TA)	E2-C Ab (aa 209–365) (detects both E2-TA and E8^E2)	Cells (%)
HFK-no virus	Background speckles	None	All
HFK-HPV16 E8^E2 mt	Throughout	Throughout	85
HFK-HPV16	Throughout	Throughout	26
HFK-HPV16	Satellite	Satellite	22
HFK-HPV16	Satellite	Throughout	22

[a]aa, amino acids.

proteins repress transcription of replicating viral DNA internal to the foci (though possibly by independent mechanisms), thus ensuring that transcription is restricted to the surface. Attempts to detect a direct interaction between these factors have been unsuccessful, and the proteins (or their recruited repressors) do not completely colocalize (e.g., Fig. 10; macroH2A1 and SMRT). Therefore, we conclude that although macroH2A1 is only recruited to HPV replication foci in cells that express the E8^E2 protein, as yet no direct association has been identified.

DISCUSSION

In this study, we show that the variant histone macroH2A is recruited to HPV replication foci, and we investigated the potential roles of this protein in the productive stage of the viral life cycle. Using ChIPseq, we find that macroH2A1 is associated with viral DNA and that this association increases in differentiated 9E cells. However, depletion of macroH2A1 in these cells had no effect on HPV31 viral DNA copy number. We also observed that depletion of macroH2A1 reduced the levels of late viral transcripts but also reduced expression of the keratinocyte differentiation markers (involucrin and filaggrin), indicating that the effect of macroH2A1 depletion on the viral transcription might be indirect. macroH2A1 is generally bound to repressed chromatin (25, 41); the majority of genes that are occupied with macroH2A1 are silent. We propose that macroH2A represses transcription of the viral DNA internal to the foci, which is undergoing replication and processing. Our data indicate that viral chromatin on the surface of the foci is transcriptionally active, so macroH2A could indirectly activate chromatin by organizing the replication foci into transcriptionally active and inactive zones.

For the most part, we observe that sites of viral replication and transcriptional regulation are spatially separated in HPV-infected cells, as RPA is localized inside the foci, while phosphorylated forms of RNA polymerase and the transcriptional regulator Brd4 are localized toward the periphery of HPV31 foci. We further propose that the spatial separation of replication and transcription compartments is regulated by association of macroH2A1 with viral chromatin (Fig. 12). It has been shown previously that in adeno-

wildtype HPV
replication focus

HPV E8^E2 mutant
replication focus

○ viral chromatin
○ active
○ macroH2A1 repressed
○ E8^E2 repressed
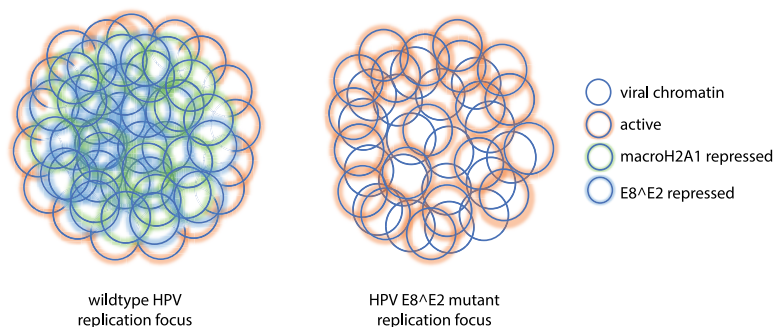
FIG 12 Model of spatial organization of an HPV replication focus in HPV16 wild-type and ΔE8^E2 genome-containing cells. On the left, HPV genomes in the center of the replication focus are associated with the viral E8^E2 and cellular macroH2A1 repressor proteins, and active chromatin is restricted to the surface of the foci. On the right, cells with HPVΔE8^E2 genomes do not express the E8^E2 protein (and so do not recruit cellular corepressors to the foci). The macroH2A1 variant histone is also absent from these foci, and active chromatin is found throughout the focus.

virus-infected cells, replication and transcription sites are spatially separated (42) and that viral replication and transcription are partitioned into different substructures within replication compartments in HSV-infected cells (43). Very little is known about the spatial organization of HPV late gene expression and virion assembly, and this is a fruitful area for future study.

The presence of Brd4 and the E2-TA protein (in addition to phosphorylated forms of RNA polymerase) on the surface of the replication foci implies that these are regions of transcriptional regulation. Brd4 is most often a positive regulator of transcription and can activate early HPV transcription (44, 45). However, for the most part, Brd4 is a transcriptional repressor in the presence of the HPV E2 protein (reviewed in reference 46). The short form of Brd4 has also been shown recently to repress late viral transcription in undifferentiated cells (47). Nevertheless, the role of Brd4 in regulating viral transcription in productive infection is not well understood, and there is evidence that it may activate the late promoter by promoting transcriptional elongation (48). We have attempted to directly detect RNA transcripts within the replication foci using RNA FISH; however, the abundance of single-stranded DNA (ssDNA) intermediates in the foci has made this inconclusive. Unlike many viruses, HPVs do not induce host transcriptional shutoff, and the vast abundance of transcription of cellular genes, in particular ribosomal DNA (rDNA), makes detection of viral transcripts using 5-ethynyl uridine (EU) labeling also very difficult. Brd4 has also been shown to ensure efficient transcriptional elongation by preventing R-loop formation and transcription-replication conflicts (49); this could be very important for a virus that must synthesize large amounts of viral DNA and late mRNA to produce progeny virus.

HPV activates the ATM DNA damage pathway, and this is required for viral genome amplification in differentiated cells (5). Various components of the DNA damage response pathway localize to HPV replication factories in differentiating CIN612-9E cells (5, 9, 12, 35). In this study, we have shown that both splice variants of histone macroH2A1, macroH2A1.1 and macroH2A1.2, are recruited to foci, which are sites of HPV DNA synthesis. Moreover, we show that macroH2A1.2 is associated with viral chromatin, and this association is increased during the productive phase of the viral life cycle. macroH2A1.2 is recruited to sites of double-strand DNA breaks, and this links the compaction of DSB-proximal chromatin to the BRCA1-dependent homologous recombination repair pathway (26). The dependence of macroH2A1 accumulation on the ATM and ATR signaling pathways at double-strand break sites and fragile sites upon replication stress suggested that the DNA damage response pathway could be involved in the recruitment of macroH2A1 to the replication viral foci (50). However, here, we show that macroH2A1 is not recruited to the replication foci in a DNA damage-dependent manner since the DNA damage-associated proteins BRCA1, 53BP1, and RAD51 localize to E8^E2 mutant viral replication foci in the absence of macroH2A1 colocalization. A recent study showed that macroH2A1 assists in RAD51 loading, and its loss results in a disbalance of BRCA1 and 53BP1 accumulation (51); however, we did not see evidence of this disbalance in HPV replication foci.

The E8^E2 protein is a repressor of HPV transcription and replication, and it has been shown to localize to E1-E2 dependent replication foci (16, 17). In support of this, we find that both E2-TA and E8^E2 also localize to replication foci generated in differentiated keratinocytes containing HPV16 genomes. Using antibodies against the E2 N-terminal domain (E2-TA only) and C-terminal domain (both E2-TA and E8^E2), we find that the E2-TA protein localizes in a satellite ring around both wild-type and E8^E2 mutant foci but is later distributed throughout, similar to what we have shown previously in transient replication foci (29). In some wild-type cells, however, we observe E2 within the foci with the C-terminal antibody but not with the N-terminal antibody, indicating that this is the E8^E2 protein. Moreover, the E8-associated corepressor protein, SMRT, also localizes within these foci, and we propose that E8^E2 localizes within the foci to restrict viral transcription (Fig. 12). macroH2A1 is also found within the foci in wild-type HPV-containing cells but is absent in E8^E2 mutant cells. We have been unable to

detect an interaction between macroH2A1 and the E8^E2 protein, and although they are both present in the interior of the replication foci, they do not completely colocalize. Future studies will investigate the relationship between these repressive proteins.

MATERIALS AND METHODS

Cell lines. CIN612-9E cell line-harboring extrachromosomal HPV31 genomes derived from CIN1 HPV31-positive patient biopsy specimen have been described (52). NIKS cells have been described previously (53). Human keratinocytes were isolated from neonatal foreskins as described previously (54). Cell lines containing replicating viral genomes were generated using HPV18 minicircle genomes (55) or either wild-type or E8^E2 mutant HPV16 genomes (56). The HPV16 E8^E2 genomes have a mutation that alters the codon for E8 residue W6 to a TAG termination codon with no change in the overlapping E1 open reading frame (ORF) amino acid sequence (56). HPV genomes were generated either by minicircle technology (55) or by removing the vector by restriction digestion and religation and were electroporated into NIKS or human foreskin keratinocytes (HFKs) with a pRSV2neo plasmid. Cells were selected for 5 days with 200 μg/ml G418 and cultured until colonies formed, at which point cells were pooled. Cells were checked by Southern blot analysis for extrachromosomal viral genomes before use.

Cell culture. All cells were cultured in Rheinwald-Green F medium (3:1 Ham's F12/Dulbecco modified Eagle medium [DMEM]-high glucose, 5% fetal bovine serum, 0.4 μg/ml hydrocortisone, 8.4 ng/ml cholera toxin, 10 ng/ml epidermal growth factor [EGF], 24 μg/ml adenine, and 6 μg/ml insulin) on lethally irradiated NIH J2 3T3 murine fibroblasts. NIH J2 3T3 mouse fibroblast cells were cultured in DMEM containing 10% newborn calf serum. Mouse feeders were exposed to 60 grays of gamma irradiation before coculture with keratinocytes. For differentiation, keratinocyte cell lines were cultured in F medium until confluent and then changed to low-calcium basal keratinocyte medium supplemented with SingleQuots (bovine pituitary extract, hydrocortisone, and epidermal growth factor) (Lonza Corporation). After 24 h, the medium was changed to basal medium supplemented with 1.5 mM calcium chloride, and the cells were cultured for 5 days. To obtain optimal replication foci for *in situ* studies, HFKs containing HPV16 E8^E2 genomes were undifferentiated, and cells with wild-type HPV16 genome were differentiated. However, the differentiation protocol did not affect the results obtained.

SiRNA transfections. For transient transfection with siRNA, CIN612-9E cells were plated on lethally irradiated J2/3T3 mouse fibroblasts and cultured overnight. After 24 h, cells were transfected either with siRNA against nontargeting control (D-00181a0-10-20, Dharmacon) or against macroH2A1 (E-011964-00-0005, Dharmacon). Transfections were carried out according to the manufacturer's protocol. Briefly, siRNAs were mixed with Lipofectamine RNAiMAX transfection reagent (Thermo Fisher Scientific) in Opti-MEM medium and added to cells at a final concentration of 20 nM. Cells were incubated with siRNA for the indicated time periods before feeders were removed and cells were harvested for further experimentation.

Transient transfection of expression plasmids. NIKS cells were transfected with pSG neo alone, pSG HPV16E2, and pSG HPV16E8^E2 HA using Fugene 6 according to the manufacturer's instructions. Plasmids pSG HPV16E2 and pSG HPV16E8^E2 HA were kindly provided by Frank Stubenrauch.

Viral genome copy number. Total cellular DNA was isolated from growing or differentiated CIN612-9E cells using the DNeasy blood and tissue kit (Qiagen) at the times indicated in the figures. Then, 1 to 5 ng of DNA was analyzed by qPCR using 300 nM primers and SYBR green master mix (Roche AG) using a QuantStudio 7 Flex real-time PCR system (Applied Biosystems). The primers are listed in Table S1.

Southern blot analysis. Total DNA was isolated from CIN612-9E cells using the DNeasy blood and tissue kit (Qiagen). DNA (2 μg) was digested with either a single-cut linearizing enzyme (HindIII) for the HPV genome or with a noncutter (BamHI) to linearize cellular DNA. After digestion, samples were separated on a 0.8% agarose-Tris-acetate-EDTA (TAE) gel and transferred onto nylon membranes using a Turbo Blotter (GE Healthcare). Membranes were UV cross-linked (120 mJ/cm^2), dried, and prehybridized in hybridization buffer (3× SSC [1× SSC is 0.15 M NaCl plus 0.015 M sodium citrate], 2% SDS, 5× Denhardt's solution, 0.2 mg/ml sonicated salmon sperm DNA) for 1 h. The membrane was hybridized overnight with 25 ng (^{32}P)-dCTP-labeled HPV31 DNA probe in hybridization buffer. The membrane was washed in 0.1% SDS/0.1× SSC, and hybridized DNA was visualized and quantitated by phosphor-imaging on a Typhoon scanner (GE Healthcare). The ^{32}P-radiolabeled probe was generated from a plasmid containing the entire HPV16 genome by radiolabeling using a Random Prime labeling kit (Roche).

RNA extraction and qPCR of viral and cellular transcripts. Total RNA was extracted using an RNeasy mini-RNA extraction kit (Qiagen). RNA concentration was determined using a Nanodrop 1000 spectrophotometer (Life Technologies). RNA integrity was checked by capillary electrophoresis on a 2100 bioanalyzer system using RNA 6000 nano kits (Agilent Technologies). Reverse transcription reactions were carried out with a Transcriptor first-strand synthesis kit (Roche AG) according to the manufacturer's protocol. mRNA expression of the indicated genes was analyzed with a QuantStudio 7 Flex real-time PCR system (Applied Biosystems) using SYBR green master mix. Cloned cDNA plasmids (2.5×10^5 to 2.5×10^{-2} fg) were included in each run to generate a standard curve. Cloned cDNA standards for the HPV31 spliced mRNAs, including E1^E4 (nt 857 to 877^3,292 to 3,296), E6*I (nt 186 to 210^413 to 416), and L1 (nt 3,562 to 3,590^5,552 to 5,554) and for the cellular genes involucrin, filaggrin, and cyclophilin A were described previously (57). The relative expression of macroH2A1.1 and macroH2A1.2 was calculated with the $2^{-\Delta\Delta CT}$ method. The primers used are listed in Table S1 and were described previously (26).

Indirect immunofluorescence (IF) and image processing. CIN612-9E or HFKs were cultured on glass coverslips and fixed with 4% paraformaldehyde in phosphate-buffered saline (PBS). After fixation, the cells were permeabilized with 0.5% Triton X-100 in PBS and blocked in 5% (vol/vol) normal donkey serum (Jackson Immunoresearch). Cells were incubated with primary antibodies at 37°C for 1 h. Primary

antibodies used for IF were macroH2A1.1 rabbit monoclonal (Cell Signaling, 12455; dilution, 1:100), macroH2A1.2 mouse monoclonal (Millipore, MABE61; dilution, 1:100), H2A rabbit polyclonal (Abcam, ab 18255; dilution, 1:100), H3 rabbit polyclonal (Abcam, ab 1791; dilution, 1:100), H4 rabbit polyclonal (Abcam, ab10158; dilution, 1:100), RPA rat monoclonal (Cell Signaling, 2208; dilution, 1:250), γH2AX mouse monoclonal (Millipore, 05-636; dilution, 1:100), BRCA1 mouse monoclonal (Santa Cruz sc-6954; dilution, 1:100), RAD51 mouse monoclonal (Abcam, ab-213; dilution, 1:100), 53BP1 rabbit polyclonal (ab 21083; dilution, 1:200), RNA Pol II Ser 2 rabbit monoclonal (Abcam, ab 5095; dilution, 1:100), RNA Pol II Ser 5 mouse monoclonal (Abcam, ab5408; dilution, 1:100), H3 acetyl K9/18 rabbit polyclonal (Upstate [Millipore]; dilution, 1:100), E2 HPV16 N-terminal sheep polyclonal (Iain Morgan/Joanna Parish; dilution, 1:200) (58), E2 HPV16 C-terminal rabbit polyclonal (Francoise Thierry; dilution, 1:100) (59), SMRT rabbit polyclonal (Bethyl Laboratories; dilution, 1:100) (29), Brd4 (CW152; dilution, 1: 300) (29), PCNA mouse mono-clonal (Santa Cruz, sc-28250; dilution, 1:100), and H3K27 dimethyl/trimethyl mouse monoclonal (Abcam, ab 6147; dilution, 1:100. The macroH2A1.1 and macroH2A1.2 antibodies were validated by depleting macroH2A1.2 using siRNA transfection (Fig. S2). After primary antibody incubation, the cells were washed three times with PBS and incubated with the secondary antibodies (Alexa 488, Alexa 594, Rhodamine Red-X, and Alexa 647 conjugated to the target species [Jackson Immunoresearch]) at 37°C for 40 min. Nuclei were stained with DAPI, and coverslips were mounted using 10 μl of Prolong Gold (Life Technologies). All Images were acquired with TCS-SP5 or TCS-SP8 laser scanning confocal micro-scopes (Leica Microsystems) using a ×63 oil immersion objective (numerical aperture [NA] 1.4). All 2D images were grabbed as a single optical slice for all the experiments unless otherwise mentioned. 3D images were deconvolved using Huygens Essential (version 20.04, Scientific Volume Imaging B.V.) using theoretical point spread function (PSF) and manual background subtraction. All images were processed using LASAF Lite (Leica microsystems) or Imaris (version 9.6.0, Bitplane).

Combined immunofluorescence and *in situ* hybridization (IF-FISH). Paraformaldehyde-fixed cells were stained with macroH2A1.2 antibody as described above. After immunostaining, cells were fixed for the second time with methanol and acetic acid solution (3:1 vol/vol) at room temperature for 10 min, fol-lowed by fixation with 2% paraformaldehyde (PFA) for 1 min. Coverslips were treated with RNace-iT cocktail (1:1,000 dilution; Agilent Technologies) at 37°C for 1 h and dehydrated in a 70%, 90%, and 100% ethanol series for 3 min each and air dried. DNA FISH probes were prepared using the FISH-Tag DNA multicolor labeling kit (Life Technologies) according to the manufacturer's protocol. Hybridization was performed overnight in 1× hybridization buffer (Empire Genomics) with 50 to 75 ng of labeled probe DNA at 37°C. Slides were washed at room temperature with 1× phosphate-buffered detergent (PBD; MP Biosciences), followed by washing with wash buffer (0.5× SSC, 0.1% SDS) at 65°C. Nuclei were stained with DAPI, coverslips were mounted using Prolong Gold (Life Technologies), and images were captured using a TCS-SP5 or TCS-SP8 microscope (Leica Microsystems).

Image analysis. To measure enrichment of macroH2A1 at the viral replication foci, ImageJ (Java ver-sion 1.8.0_112) was used to define regions of interest (ROIs) around the viral replication foci (around the RPA signal) and equivalent nonreplication foci regions in the nucleus and cytoplasm. The mean fluores-cence intensity within the ROIs was measured for macroH2A1. Background intensity values (cytoplasm) were subtracted, and the ratio of intensity within the replication foci to nonreplication foci was calcu-lated. 3D images were collected as noted in the figure legends. 3D images were deconvolved using Huygens Essential (20.04 Scientific Volume Imaging B.V.). All images were processed using LASAF Lite (Leica Microsystems) and Imaris (version 9.6.0, Bitplane). For the colocalization analysis, 3D images were first deconvolved in Huygens Essential. Replication foci ROI were defined by RPA signal using the surface masking technique in Imaris. Then colocalization analysis was performed and the Pearson's coefficient was calculated in replication foci using Imaris.

Chromatin immunoprecipitation. Chromatin from growing and differentiated CIN612-9E cells was prepared as described previously (57, 60). Briefly, following formaldehyde fixation and glycine quenching, cells were resuspended in cell lysis buffer I to isolate nuclei (50 mM HEPES KOH pH 7.5, 140 mM NaCl, 1 mM EDTA, 10% glycerol, 0.5% NP-40, 0.5% Triton X-100). Lysates were prepared from isolated nuclei as described in Stepp et al., (57). Lysates were sonicated using an ultrasonicator water bath (Bioruptor, Diagenode). A Southern blot analysis was performed to ensure the optimal shearing of viral chromatin (200- to 500-bp fragments). DNA shearing was also measured by agarose gel electrophoresis. For immuno-precipitations, 20 μg of chromatin was incubated with either 3 μg of rabbit IgG (ChromPure), macroH2A1.2 (Millipore, MABE61), or Brd4 (Bethyl, A301-985A100) antibodies overnight at 4°C. Immune complexes were collected using 30 μl protein G Dynabeads (Invitrogen). DNA was purified using a ChIP DNA Clean and Concentrator kit (Zymo Research). Immunoprecipitated HPV chromatin was quantified by comparison with an HPV31 plasmid standard curve using the QuantStudio 7 Flex real-time PCR system.

Chromatin immunoprecipitation and Illumina sequencing. Chromatin from growing and differen-tiated CIN612-9E was processed as described above. ChIP and input libraries were sequenced (2 × 150-bp paired-end reads) using the Illumina HiSeq 4000 platform (Genomics Resource Center, Institute for Genome Sciences, University of Maryland). Reads were trimmed with Cutadapt version 1.18 (61). All reads aligning to the Encode hg19 v1 blacklist regions (62) were identified by alignment with the Burrows-Wheeler Aligner (BWA) version 0.7.17 (63) and removed with Picard SamToFastq (the Picard toolkit. https://broadinstitute.github.io/picard/). The remaining reads were aligned to an hg19 reference genome with an additional HPV31 chromosome (GenBank ID J04353.1) using BWA. Reads with a mapQ score of less than 6 were removed with SAMtools version 1.6 (64), and PCR duplicates were removed with Picard MarkDuplicates. Replicate ChIP samples were merged after deduplication using SAMtools. Data were converted into bigwigs for viewing and normalized by reads per genomic content (RPGC) using deepTools version 3.0.1 (65) using the following parameters: –binSize 25 –smoothLength 75 –effectiveGenomeSize

2700000000 –centerReads –normalizeUsing RPGC. RPGC-normalized input values were subtracted from RPGC-normalized ChIP values of matching cell type genome-wide using DeepTools with –binSize 25. Here, the human genome reads were used only to normalize the viral read counts, and the full analysis of macroH2A binding to the human genome will be published elsewhere.

Western blot analysis. Medium was removed and J2 fibroblast feeder cells were removed with Versene (Thermo Fisher). Keratinocyte monolayers were rinsed with ice-cold PBS. Growing and differentiated cells were lysed on the plate with 1 ml SDS lysis buffer (1% wt/vol SDS, 10 mM Tris-HCl pH 8, 1 mM EDTA pH 8) heated to 95°C. After the plate was scraped, samples were transferred to a low-protein-binding microcentrifuge tube and sonicated using a Bioruptor (30 s on, 30 s off, for 6 cycles at high power). After sonication, samples were heated at 95°C for 10 min in a heat block and centrifuged at $16,100 \times g$ for 5 min to remove any debris. Then, 10 to 20 μg total protein was supplemented with 50 mM DTT and 4$\times$ lithium dodecyl sulfate (LDS) sample buffer (Life Technologies). Samples were heated to 70°C for 10 min and cooled to room temperature, and proteins were separated by SDS-PAGE on 4 to 12% NuPage gradient gels (Life Technologies). Proteins were transferred overnight onto polyvinylidene difluoride (PVDF) membrane. Western blotting was performed using the following antibodies: anti-macroH2A1.1 (Cell Signaling, 12455; dilution, 1:1,000), anti-macroH2A1.2 (Millipore, MABE61; dilution, 1:1,000), anti-Histone H3 (Upstate Millipore 07-690; dilution, (1:10,000). Horseradish peroxidase conjugated secondary antibodies (anti-rabbit [Invitrogen 31460] and anti-mouse [Invitrogen, 31430]) were used at 1:10,000 dilutions. The antibodies were detected using chemiluminescent reagents (SuperSignal Dura Western Detection), and the signal was detected and quantitated using a G:Box (Syngene).

SUPPLEMENTAL MATERIAL

Supplemental material is available online only.

FIG S1, PDF file, 2 MB.
FIG S2, PDF file, 1.1 MB.
FIG S3, PDF file, 1.1 MB.
FIG S4, PDF file, 2.3 MB.
FIG S5, PDF file, 2.2 MB.
FIG S6, PDF file, 2 MB.
TABLE S1, DOCX file, 0.02 MB.

ACKNOWLEDGMENTS

REFERENCES

1. de Martel C, Plummer M, Vignat J, Franceschi S. 2017. Worldwide burden of cancer attributable to HPV by site, country and HPV type. Int J Cancer 141:664–670. https://doi.org/10.1002/ijc.30716.
2. Howley PM, Pfister HJ. 2015. Beta genus papillomaviruses and skin cancer. Virology 479–480:290–296. https://doi.org/10.1016/j.virol.2015.02.004.
3. Doorbar J, Egawa N, Griffin H, Kranjec C, Murakami I. 2015. Human papillomavirus molecular biology and disease association. Rev Med Virol 25 Suppl 1:2–23. https://doi.org/10.1002/rmv.1822.
4. Bedell MA, Hudson JB, Golub TR, Turyk ME, Hosken M, Wilbanks GD, Laimins LA. 1991. Amplification of human papillomavirus genomes in vitro is dependent on epithelial differentiation. J Virol 65:2254–2260. https://doi.org/10.1128/JVI.65.5.2254-2260.1991.
5. Moody CA, Laimins LA. 2009. Human papillomaviruses activate the ATM DNA damage pathway for viral genome amplification upon differentiation. PLoS Pathog 5:e1000605. https://doi.org/10.1371/journal.ppat.1000605.
6. Coursey TL, McBride AA. 2019. Hitchhiking of viral genomes on cellular chromosomes. Annu Rev Virol 6:275–296. https://doi.org/10.1146/annurev-virology-092818-015716.
7. Sakakibara N, Mitra R, McBride AA. 2011. The papillomavirus E1 helicase activates a cellular DNA damage response in viral replication foci. J Virol 85:8981–8995. https://doi.org/10.1128/JVI.00541-11.

8. Fradet-Turcotte A, Bergeron-Labrecque F, Moody CA, Lehoux M, Laimins LA, Archambault J. 2011. Nuclear accumulation of the papillomavirus E1 helicase blocks S-phase progression and triggers an ATM-dependent DNA damage response. J Virol 85:8996–9012. https://doi.org/10.1128/JVI.00542-11.
9. Gillespie KA, Mehta KP, Laimins LA, Moody CA. 2012. Human papillomaviruses recruit cellular DNA repair and homologous recombination factors to viral replication centers. J Virol 86:9520–9526. https://doi.org/10.1128/JVI.00247-12.
10. Jang MK, Shen K, McBride AA. 2014. Papillomavirus genomes associate with BRD4 to replicate at fragile sites in the host genome. PLoS Pathog 10:e1004117. https://doi.org/10.1371/journal.ppat.1004117.
11. Sitz J, Blanchet SA, Gameiro SF, Biquand E, Morgan TM, Galloy M, Dessapt J, Lavoie EG, Blondeau A, Smith BC, Mymryk JS, Moody CA, Fradet-Turcotte A. 2019. Human papillomavirus E7 oncoprotein targets RNF168 to hijack the host DNA damage response. Proc Natl Acad Sci U S A 116: 19552–19562. https://doi.org/10.1073/pnas.1906102116.
12. Anacker DC, Gautam D, Gillespie KA, Chappell WH, Moody CA. 2014. Productive replication of human papillomavirus 31 requires DNA repair factor Nbs1. J Virol 88:8528–8544. https://doi.org/10.1128/JVI.00517-14.
13. Bester AC, Roniger M, Oren YS, Im MM, Sarni D, Chaoat M, Bensimon A, Zamir G, Shewach DS, Kerem B. 2011. Nucleotide deficiency promotes

genomic instability in early stages of cancer development. Cell 145: 435–446. https://doi.org/10.1016/j.cell.2011.03.044.

14. Moody CA. 2019. Impact of replication stress in human papillomavirus pathogenesis. J Virol 93:e01012-17. https://doi.org/10.1128/JVI.01012-17.

15. Stubenrauch F, Hummel M, Iftner T, Laimins LA. 2000. The E8E2C protein, a negative regulator of viral transcription and replication, is required for extrachromosomal maintenance of human papillomavirus type 31 in keratinocytes. J Virol 74:1178–1186. https://doi.org/10.1128/jvi.74.3.1178-1186.2000.

16. Dreer M, Fertey J, van de Poel S, Straub E, Madlung J, Macek B, Iftner T, Stubenrauch F. 2016. Interaction of NCOR/SMRT repressor complexes with papillomavirus E8^ E2C proteins inhibits viral replication. PLoS Pathog 12:e1005556. https://doi.org/10.1371/journal.ppat.1005556.

17. Dreer M, van de Poel S, Stubenrauch F. 2017. Control of viral replication and transcription by the papillomavirus E8^E2 protein. Virus Res 231: 96–102. https://doi.org/10.1016/j.virusres.2016.11.005.

18. Stunkel W, Bernard HU. 1999. The chromatin structure of the long control region of human papillomavirus type 16 represses viral oncoprotein expression. J Virol 73:1918–1930. https://doi.org/10.1128/JVI.73.3.1918-1930.1999.

19. Favre M, Breitburd F, Croissant O, Orth G. 1977. Chromatin-like structures obtained after alkaline disruption of bovine and human papillomaviruses. J Virol 21:1205–1209. https://doi.org/10.1128/JVI.21.3.1205-1209.1977.

20. Porter SS, Liddle JC, Browne K, Pastrana DV, Garcia BA, Buck CB, Weitzman MD, McBride AA. 2021. Histone modifications in papillomavirus virion minichromosomes. mBio 12:e03274-20. https://doi.org/10.1128/mBio.03274-20.

21. Mac M, Moody CA. 2020. Epigenetic regulation of the human papillomavirus life cycle. Pathogens 9:483. https://doi.org/10.3390/pathogens9060483.

22. Burley M, Roberts S, Parish JL. 2020. Epigenetic regulation of human papillomavirus transcription in the productive virus life cycle. Semin Immunopathol 42:159–171. https://doi.org/10.1007/s00281-019-00773-0.

23. Timinszky G, Till S, Hassa PO, Hothorn M, Kustatscher G, Nijmeijer B, Colombelli J, Altmeyer M, Stelzer EH, Scheffzek K, Hottiger MO, Ladurner AG. 2009. A macrodomain-containing histone rearranges chromatin upon sensing PARP1 activation. Nat Struct Mol Biol 16:923–929. https://doi.org/10.1038/nsmb.1664.

24. Pehrson JR, Costanzi C, Dharia C. 1997. Developmental and tissue expression patterns of histone macroH2A1 subtypes. J Cell Biochem 65:107–113. https://doi.org/10.1002/(SICI)1097-4644(199704)65:1<107::AID-JCB11>3.0.CO;2-H.

25. Gamble MJ, Frizzell KM, Yang C, Krishnakumar R, Kraus WL. 2010. The histone variant macroH2A1 marks repressed autosomal chromatin, but protects a subset of its target genes from silencing. Genes Dev 24:21–32. https://doi.org/10.1101/gad.1876110.

26. Khurana S, Kruhlak MJ, Kim J, Tran AD, Liu J, Nyswaner K, Shi L, Jailwala P, Sung M-H, Hakim O, Oberdoerffer P. 2014. A macrohistone variant links dynamic chromatin compaction to BRCA1-dependent genome maintenance. Cell Rep 8:1049–1062. https://doi.org/10.1016/j.celrep.2014.07.024.

27. Kim J, Sturgill D, Sebastian R, Khurana S, Tran AD, Edwards GB, Kruswick A, Burkett S, Hosogane EK, Hannon WW, Weyemi U, Bonner WM, Luger K, Oberdoerffer P. 2018. Replication stress shapes a protective chromatin environment across fragile genomic regions. Mol Cell 69:36–47.e7. https://doi.org/10.1016/j.molcel.2017.11.021.

28. Zhang R, Poustovoitov MV, Ye X, Santos HA, Chen W, Daganzo SM, Erzberger JP, Serebriiskii IG, Canutescu AA, Dunbrack RL, Pehrson JR, Berger JM, Kaufman PD, Adams PD. 2005. Formation of MacroH2A-containing senescence-associated heterochromatin foci and senescence driven by ASF1a and HIRA. Dev Cell 8:19–30. https://doi.org/10.1016/j.devcel.2004.10.019.

29. Sakakibara N, Chen D, Jang MK, Kang DW, Luecke HF, Wu SY, Chiang CM, McBride AA. 2013. Brd4 is displaced from HPV replication factories as they expand and amplify viral DNA. PLoS Pathog 9:e1003777. https://doi.org/10.1371/journal.ppat.1003777.

30. Iftner T, Haedicke-Jarboui J, Wu SY, Chiang CM. 2017. Involvement of Brd4 in different steps of the papillomavirus life cycle. Virus Res 231: 76–82. https://doi.org/10.1016/j.virusres.2016.12.006.

31. Donati B, Lorenzini E, Ciarrocchi A. 2018. BRD4 and Cancer: going beyond transcriptional regulation. Mol Cancer 17:164. https://doi.org/10.1186/s12943-018-0915-9.

32. Spink KM, Laimins LA. 2005. Induction of the human papillomavirus type 31 late promoter requires differentiation but not DNA amplification. J Virol 79:4918–4926. https://doi.org/10.1128/JVI.79.8.4918-4926.2005.

33. Creppe C, Janich P, Cantariño N, Noguera M, Valero V, Musulén E, Douet J, Posavec M, Martín-Caballero J, Sumoy L, Di Croce L, Benitah SA, Buschbeck M. 2012. MacroH2A1 regulates the balance between self-renewal and differentiation commitment in embryonic and adult stem cells. Mol Cell Biol 32: 1442–1452. https://doi.org/10.1128/MCB.06323-11.

34. Straub E, Dreer M, Fertey J, Iftner T, Stubenrauch F. 2014. The viral E8^E2C repressor limits productive replication of human papillomavirus 16. J Virol 88:937–947. https://doi.org/10.1128/JVI.02296-13.

35. Moody C. 2017. Mechanisms by which HPV induces a replication competent environment in differentiating keratinocytes. Viruses 9:261. https://doi.org/10.3390/v9090261.

36. Chappell WH, Gautam D, Ok ST, Johnson BA, Anacker DC, Moody CA. 2015. Homologous recombination repair factors Rad51 and BRCA1 are necessary for productive replication of human papillomavirus 31. J Virol 90:2639–2652. https://doi.org/10.1128/JVI.02495-15.

37. Angelov D, Molla A, Perche PY, Hans F, Cote J, Khochbin S, Bouvet P, Dimitrov S. 2003. The histone variant macroH2A interferes with transcription factor binding and SWI/SNF nucleosome remodeling. Mol Cell 11: 1033–1041. https://doi.org/10.1016/s1097-2765(03)00100-x.

38. Hsin JP, Manley JL. 2012. The RNA polymerase II CTD coordinates transcription and RNA processing. Genes Dev 26:2119–2137. https://doi.org/10.1101/gad.200303.112.

39. Dey A, Chitsaz F, Abbasi A, Misteli T, Ozato K. 2003. The double bromodomain protein Brd4 binds to acetylated chromatin during interphase and mitosis. Proc Natl Acad Sci U S A 100:8758–8763. https://doi.org/10.1073/pnas.1433065100.

40. Jang MK, Mochizuki K, Zhou M, Jeong HS, Brady JN, Ozato K. 2005. The bromodomain protein Brd4 is a positive regulatory component of P-TEFb and stimulates RNA polymerase II-dependent transcription. Mol Cell 19: 523–534. https://doi.org/10.1016/j.molcel.2005.06.027.

41. Buschbeck M, Uribesalgo I, Wibowo I, Rue P, Martin D, Gutierrez A, Morey L, Guigo R, Lopez-Schier H, Di Croce L. 2009. The histone variant macroH2A is an epigenetic regulator of key developmental genes. Nat Struct Mol Biol 16:1074–1079. https://doi.org/10.1038/nsmb.1665.

42. Pombo A, Ferreira J, Bridge E, Carmo-Fonseca M. 1994. Adenovirus replication and transcription sites are spatially separated in the nucleus of infected cells. EMBO J 13:5075–5085. https://doi.org/10.1002/j.1460-2075.1994.tb06837.x.

43. Li Z, Fang C, Su Y, Liu H, Lang F, Li X, Chen G, Lu D, Zhou J. 2016. Visualizing the replicating HSV-1 virus using STED super-resolution microscopy. Virol J 13:65. https://doi.org/10.1186/s12985-016-0521-7.

44. McKinney CC, Kim MJ, Chen D, McBride AA. 2016. Brd4 activates early viral transcription upon human papillomavirus 18 infection of primary keratinocytes. mBio 7:e01644-16. https://doi.org/10.1128/mBio.01644-16.

45. Morse MA, Balogh KK, Brendle SA, Campbell CA, Chen MX, Furze RC, Harada IL, Holyer ID, Kumar U, Lee K, Prinjha RK, Rudiger M, Seal JT, Taylor S, Witherington J, Christensen ND. 2018. BET bromodomain inhibitors show anti-papillomavirus activity in vitro and block CRPV wart growth in vivo. Antiviral Res 154:158–165. https://doi.org/10.1016/j.antiviral.2018.03.012.

46. McBride AA, Warburton A, Khurana S. 2021. Multiple roles of Brd4 in the infectious cycle of human papillomaviruses. Front Mol Biosci 8:725794. https://doi.org/10.3389/fmolb.2021.725794.

47. Yigitliler A, Renner J, Simon C, Schneider M, Stubenrauch F, Iftner T. 2021. BRD4S interacts with viral E2 protein to limit human papillomavirus late transcription. J Virol 95:e02032-20. https://doi.org/10.1128/JVI.02032-20.

48. Songock WK, Scott ML, Bodily JM. 2017. Regulation of the human papillomavirus type 16 late promoter by transcriptional elongation. Virology 507:179–191. https://doi.org/10.1016/j.virol.2017.04.021.

49. Edwards DS, Maganti R, Tanksley JP, Luo J, Park JJH, Balkanska-Sinclair E, Ling J, Floyd SR. 2020. BRD4 prevents R-loop formation and transcription-replication conflicts by ensuring efficient transcription elongation. Cell Rep 32:108166. https://doi.org/10.1016/j.celrep.2020.108166.

50. Kim J, Oberdoerffer P, Khurana S. 2018. The histone variant macroH2A1 is a splicing-modulated caretaker of genome integrity and tumor growth. Mol Cell Oncol 5:e1441629. https://doi.org/10.1080/23723556.2018.1441629.

51. Xu X, Ni K, He Y, Ren J, Sun C, Liu Y, Aladjem MI, Burkett S, Finney R, Ding X, Sharan SK, Muegge K. 2021. The epigenetic regulator LSH maintains fork protection and genomic stability via MacroH2A deposition and RAD51 filament formation. Nat Commun 12:3520. https://doi.org/10.1038/s41467-021-23809-2.

52. Hummel M, Hudson JB, Laimins LA. 1992. Differentiation-induced and constitutive transcription of human papillomavirus type 31b in cell lines containing viral episomes. J Virol 66:6070–6080. https://doi.org/10.1128/JVI.66.10.6070-6080.1992.

53. Allen-Hoffmann BL, Schlosser SJ, Ivarie CA, Sattler CA, Meisner LF, O'Connor SL. 2000. Normal growth and differentiation in a spontaneously immortalized near-diploid human keratinocyte cell line, NIKS. J Invest Dermatol 114: 444–455. https://doi.org/10.1046/j.1523-1747.2000.00869.x.

54. Chapman S, Liu X, Meyers C, Schlegel R, McBride AA. 2010. Human keratinocytes are efficiently immortalized by a Rho kinase inhibitor. J Clin Invest 120:2619–2626. https://doi.org/10.1172/JCI42297.

55. Henno L, Tombak EM, Geimanen J, Orav M, Ustav E, Ustav M. 2017. Analysis of human papillomavirus genome replication using two- and three-dimensional agarose gel electrophoresis. Curr Protoc Microbiol 45: 14B.10.1–14B.10.37. https://doi.org/10.1002/cpmc.28.

56. Lace MJ, Anson JR, Thomas GS, Turek LP, Haugen TH. 2008. The E8-E2 gene product of human papillomavirus type 16 represses early transcription and replication but is dispensable for viral plasmid persistence in keratinocytes. J Virol 82:10841–10853. https://doi.org/10.1128/JVI.01481-08.

57. Stepp WH, Stamos JD, Khurana S, Warburton A, McBride AA. 2017. Sp100 colocalizes with HPV replication foci and restricts the productive stage of the infectious cycle. PLoS Pathog 13:e1006660. https://doi.org/10.1371/journal.ppat.1006660.

58. Gauson EJ, Donaldson MM, Dornan ES, Wang X, Bristol M, Bodily JM, Morgan IM. 2015. Evidence supporting a role for TopBP1 and Brd4 in the initiation but not continuation of human papillomavirus 16 E1/E2-mediated DNA replication. J Virol 89:4980–4991. https://doi.org/10.1128/JVI.00335-15.

59. Xue Y, Bellanger S, Zhang W, Lim D, Low J, Lunny D, Thierry F. 2010. HPV16 E2 is an immediate early marker of viral infection, preceding E7 expression in precursor structures of cervical carcinoma. Cancer Res 70: 5316–5325. https://doi.org/10.1158/0008-5472.CAN-09-3789.

60. Dooley KE, Warburton A, McBride AA. 2016. Tandemly integrated HPV16 can form a Brd4-dependent super-enhancer-like element that drives transcription of viral oncogenes. mBio 7:e01446-16. https://doi.org/10.1128/mBio.01446-16.

61. Martin M. 2011. Cutadapt removes adapter sequences from high-throughput sequencing reads. EMBnet J 17:10–12. https://doi.org/10.14806/ej.17.1.200.

62. The ENCODE Project Consortium. 2012. An integrated encyclopedia of DNA elements in the human genome. Nature 489:57–74. https://doi.org/10.1038/nature11247.

63. Li H, Durbin R. 2009. Fast and accurate short read alignment with Burrows-Wheeler transform. Bioinformatics 25:1754–1760. https://doi.org/10.1093/bioinformatics/btp324.

64. Li H, Handsaker B, Wysoker A, Fennell T, Ruan J, Homer N, Marth G, Abecasis G, Durbin R, 1000 Genome Project Data Processing Subgroup. 2009. The Sequence Alignment/Map format and SAMtools. Bioinformatics 25:2078–2079. https://doi.org/10.1093/bioinformatics/btp352.

65. Ramirez F, Ryan DP, Gruning B, Bhardwaj V, Kilpert F, Richter AS, Heyne S, Dundar F, Manke T. 2016. deepTools2: a next generation web server for deep-sequencing data analysis. Nucleic Acids Res 44:W160–W165. https://doi.org/10.1093/nar/gkw257.